

Large Angle Particle DO Group

M.R. Adams, ^(s) L. Ahrens, ^(a) S. Aronson, ^(a) J. Callas, ^(b), D. Cutts, ^(b)
 R. Dixon, ^(f) R. Engelmann, ^(s) D. Finley, ^(f) G. Finocchiaro, ^(s)
 P. Franzini, ^(c) B. Gibbard, ^(a) M.L. Good, ^(s) P.D. Grannis, ^(s) M. Harrison, ^(f)
 D. Hedin, ^(s) J. Horstkotte, ^(s) H. Jostlein, ^(f) T. Kafka, ^(s) J. Kirz, ^(s)
 R.E. Lanou, ^(b) J. Lee-Franzini, ^(s) M. Marx, ^(s) P. Mazur ^(f) R.L. McCarthy, ^(s)
 B.G. Pope, ^(p) C. Rad, ^(f) R.D. Schamberger, ^(s) T. Shinkawa, ^(b) P. Tuts, ^(s)
 H. Weisberg, ^(a) P. Yamin ^(a)

(Brookhaven ^(a) - Brown ^(b) - Columbia ^(c) - Fermilab ^(f) -
 Princeton ^(p) - Stony Brook ^(s) Collaboration)

Spokesmen: P. Grannis
 M. Marx
 State University of New York
 Stony Brook, NY 11794
 (516 246-7968 - PG
 -4033 - MM
 -6105 - Secretary)

I. Introduction

We propose an experiment for the DO area in the $\bar{p}p$ Collider at Fermilab. This experiment, dubbed LAPDOG, is based on a non-magnetic, large solid-angle array of high resolution electromagnetic calorimeters. Its central feature is a set of highly segmented lead glass detectors. The primary physics goals are the study of massive electron-positron pair production and of large transverse momentum π^0 , photon and electron production.

Such an experiment has the advantages of being relatively compact and of providing a rather well focussed method for studying certain well defined issues. Primarily because of its omission of a central magnetic field, it will not address many of the questions open to a large facility experiment; because of its small size it can afford to do a better job in certain areas than the more global experiment. We note that previous experiments of similar configuration, scope and emphasis have been remarkably successful in colliding beam machines. In particular, R103 (CERN-Columbia-Rockefeller) and its successors at the ISR, and R806 (Athens-Brookhaven-CERN-Syracuse-Yale) at the ISR have had a strong impact on understanding of hadronic interactions. Similarly, the Crystal Ball (Cal Tech-Harvard-Princeton-Stanford-SLAC) and the CUSB experiment (Columbia-LSU-Max Planck-Stony Brook) have made important discoveries at e^+e^- machines. A common feature of these experiments is the use of high resolution electromagnetic detection. LAPDOG seeks to exploit this same philosophy in order to examine some of the new issues opened up by the Fermilab Collider - exploration of the properties of intermediate vector bosons, continuation of the search for massive quark-antiquark bound states, and extension

of large- p_T particle production to the 75-100 GeV/c regime. We believe that this experiment, with its rather simple geometry and event analysis properties, with its superior energy resolution for electrons and photons, and with its relatively low cost, affords an attractive complement to the large scale, general purpose magnetic experiment now being built.

II. Physics Goals

The most fundamental questions known today which will be addressed at the Collider concern the characteristics of the intermediate vector bosons. If these states are indeed those expected in the standard theory, we may anticipate some exciting glimpses of their properties from the CERN $\bar{p}p$ Collider. There will remain however many important questions. In particular, the decay width of the Z^0 , detailed studies of Z^0 production cross-section dependences on p_T and x (and the related insight into the hadronic constituent structure), and the observation of parity violating effects in hadronic collisions and the resulting information on the short-distance space-time properties of the electroweak interaction are all likely to be unresolved issues at the time of the Fermilab Collider start-up.

Another long-standing question of fundamental significance is the nature of the forces and constituents at the smallest distance scales. Experiments addressing this question have repeatedly shown surprising results. The high energy and luminosity of the Collider will allow a very large increase in the range of transverse momentum over which particle production can be measured. We should remember that it is p_T (and not some scaling variable) which is conjugate to distance. Studies at one fifth of the distance scale previously resolved are sure to provide interesting physics.

Specifically, the goals we have had in mind in designing an experiment are the following:

1) Z^0 properties

In a 100 day experiment with $\mathcal{L} = 2 \times 10^{29} \text{ cm}^{-2} \text{ sec}^{-1}$ ($\int \mathcal{L} dt \equiv \mathcal{L} = 1.7 \times 10^{36} \text{ cm}^{-2}$) -- the standard chosen for this proposal-- we expect 470 events detected for e^+e^- . With the energy resolution afforded by lead-glass we expect a

mass resolution at the Z^0 of $\pm 1\%$ or $\pm 0.9 \text{ GeV}/c$. This is to be compared with the expected¹ width of the Z^0 , $\Gamma_Z/2 = 1.5 \text{ GeV}$. We propose to measure the physical width, Γ_Z to a precision $\delta\Gamma_Z = 230 \text{ MeV}$ with these events. This measurement is important in determining the various quark and leptonic couplings to the Z^0 . Together with experiments measuring Z^0 decays into quarks it allows the determination of partial widths of Z^0 decays into leptons and quarks. More importantly, within the context of the standard model, measurement of Γ_Z gives a determination of the number of neutrino species, and hence an indication of the number of fermion generations. Current estimates give a contribution of 180 MeV to Γ_Z for each new species of neutrino.

This relatively large number of clean Z^0 events will allow us to measure Z^0 production out to $p_T \sim 25 \text{ GeV}/c$. Present guesses are that the average p_T ($\langle p_T^2 \rangle^{1/2}$) $\sim 10 \text{ GeV}$, and that these large values are controlled by QCD effects. They are not easily calculable at this time. Conversely, measurement of $d\sigma/dp_T$ for Z^0 production will have important consequences for our understanding of QCD. We note that the test of QCD in the intermediate boson cross-sections, where we invoke $\alpha_s(m_Z^2)$, may well be more incisive than current studies at much lower q^2 .

The study of x -distributions of Z^0 production will contain the same degree of richness as current experimentation on the production of e^+e^- by the Drell-Yan mechanism.² The higher energy of the $\bar{p}p$ Collider allows us to explore the non-scaling (energy-dependent) corrections expected from QCD.

2) Continuum dielectron studies and resonance searches

The study of dilepton production in hadronic collisions has contributed greatly to our knowledge of the substructure of hadrons. The framework of understanding - annihilation of quark-antiquark into vector boson with subsequent

materialization into lepton pair and with modifications due to higher-order QCD corrections - is basically accepted. However a number of open questions remain, largely related to the strength and type of corrections which must be applied to the basic process. Owing to the large $\sqrt{s} \approx 2000$ GeV at the Collider, the range of $\sqrt{\tau} \equiv M_{ee}/\sqrt{s}$ to be explored will be confined to $\sqrt{\tau} < 0.02$. It is precisely in this range where the QCD non-scaling corrections are expected to be most strongly felt, and where experimental information is sorely needed on the magnitude of dilepton production, as well as its p_T , $\sqrt{\tau}$ and x dependences. We emphasize that the same QCD corrections which serve to increase the Drell-Yan production at small $\sqrt{\tau}$ also give a broad p_T distribution. It is thus important to retain good efficiency for lepton pair production out to large p_T . Based upon fits to dimuon production at the ISR³, we expect dielectron rates for LAPDOG at the level of 10 events/GeV/c² for 30 GeV/c² pairs within our standard \int_L exposure. Significant departures from scaling at low $\sqrt{\tau}$ could raise the upper limit of observable masses to 40 GeV/c².

Production of vector meson states in hadronic collisions offers a somewhat complementary view of constituent structure to that given by Drell Yan production. Instead of formation of the pair from an initial state $q\bar{q}$, the vector states are produced dominantly by gluon mechanisms; for example $gg \rightarrow V g$ or $gq \rightarrow \chi q$ with $\chi \rightarrow V$. There is thus no a-priori reason to expect that the x and p_T dependences of V production will be similar to those for Drell-Yan pairs. The puzzle at present is that these dependences, for T , ψ , and ϕ , are indeed similar to continuum pairs. Clearly, extension of V -production data to the non-scaling small $\sqrt{\tau}$ regime will be most interesting. The expected differences in quark and gluon distributions at small x should produce interesting departures

in the two types of dilepton production spectra. LAPDOG proposes to explore ψ and T production at these low \sqrt{s} values; in our standard exposure of $\int \mathcal{L}$, we expect some 300 detected $T \rightarrow e^+e^-$ events and 12,000 $\psi \rightarrow e^+e^-$ events.

It is also widely surmised that a new vector state involving hidden truth will be found. LAPDOG would expect to see a signal of 10 events from $(\bar{t}t) \rightarrow e^+e^-$ at a mass of 55 GeV/c, over a background of about 1 event within the mass resolution interval, contributed from the tail of the Z^0 and from Drell-Yan production; larger signals result for lower $(\bar{t}t)$ masses.

3) Single electron spectra and $W^\pm \rightarrow e^\pm \nu$

It is generally believed that detection of the W^\pm through observation of the Jacobian peak in e^\pm production will be difficult. In addition to electrons from W^\pm , backgrounds to single electron production above $p_T = 25$ GeV/c include direct electron production (from charm, beauty etc. decays) and misidentified hadron background, as well as electrons from $Z^0 \rightarrow e^+e^-$ in which the other member of the pair is missed. The problem is compounded by the rather broad p_T distribution expected for W^\pm production resulting in a smeared-out Jacobian peak.

In the standard $\int \mathcal{L}$ exposure for LAPDOG, we expect 1650 W^+ (or W^-) decays into a detected e^\pm with $p_T(e^\pm) > 25$ GeV/c. We estimate that the sources of background from conventional sources will not dominate the single e^\pm yields in this p_T range. Furthermore, in this experiment we detect about 90% of the $Z^0 \rightarrow e^+e^-$ decays as pairs, so the background of single e^\pm from Z^0 is an order of magnitude below the W^\pm signal.

One of the clearest signals from W^\pm production in a $\bar{p}p$ colliding beam machine is the presence of an explicit parity-violating effect involving the correlation of lepton and beam momenta. Owing to the V-A structure of the W coupling to leptons, one expects a tendency for e^+ from W^+ to emerge in the

hemisphere of the antiproton beam (and vice versa for e^- from W^-). Backgrounds to single e^\pm production are expected to be either symmetric or correlated with the same sign beam. Thus this peculiar asymmetry is a strong positive indication of W^\pm production and a test of the standard electroweak model. We propose to measure this asymmetry by inserting modest toroidal magnets in the angular interval $5^\circ \lesssim \theta \lesssim 20^\circ$ with respect to both beams. These toroids are intended to measure the sign of the e^\pm in the forward directions. If we restrict ourselves to the transverse momentum interval $15 \lesssim p_T \lesssim 35$ GeV/c, where the asymmetry is largest, we expect 75 electrons of the same sign as the beam in that hemisphere and 262 of the opposite sign. The asymmetry expected is thus -0.55 with estimated statistical error ≈ 0.05 . We emphasize that in the region covered by these sign-determining magnets, our backgrounds from hadron misidentification are expected to be minimal because of the large (~ 100 GeV/c) momentum of the detected electrons. The presence of the sign selection on both sides, coupled with the precise p_T and θ determination, should help appreciably in understanding backgrounds and measuring this asymmetry.

4) Large transverse momentum π^0 (γ) production

Measurement of single particle production cross-sections at large p_T gave one of the first confirmations of constituent substructure in hadronic interactions. Theoretical ideas and recent experiments⁴ suggest that quark-quark (and quark-gluon) scattering is the dominant mechanism even though the p_T^{-4} dependence naively predicted is not observed. The higher \sqrt{s} value for the Collider gives, at fixed p_T , a lower x_T and hence a larger cross-section. The result is that one can expect to observe single particle production out to $p_T \sim 75$ GeV/c. This is approximately five times the maximum value observed at the ISR. The resulting

improvement in resolution in probing hadrons is of general interest. In any case, such large p_T values should allow relatively clean identification of the dominant constituent scattering mechanism.

An experimentally related question is the inclusive single photon production cross-section. Here the dominant subprocesses are $q\bar{q} \rightarrow q\gamma$ and $\bar{q}q \rightarrow \gamma g$. Estimates of the γ/π^0 ratio range between 5% and 40% for $p_T \sim 50$ GeV/c. We propose to measure this ratio using a statistical method, out to $p_T \leq 50$ GeV/c.

There are two final comments pertinent to these high p_T studies. The first is an experimental one: measurement of large $p_T \pi^0(\gamma)$ can be done with a high resolution electromagnetic calorimeter on a size scale small compared with magnetic analysis of charged particles. Thus one can afford large solid angle coverage, as LAPDOG provides, with the resulting larger event sample at any given p_T . Previous experiments suggest that charged particle production is similar to π^0 production at large p_T , small x_T .

The second comment is a theoretical one: The QCD corrections to large p_T production involve knowing the coupling constant $\alpha_s(q^2)$. At presently attainable values of p_T , α_s is clearly rather large and the corrections become rather complex. We may anticipate crisper theoretical handling of higher order corrections for the p_T range studied by LAPDOG.

III. Experimental Apparatus

A. Lead Glass Calorimeters

LAPDOG is based on a detection scheme using extruded (or extrusion cast) bars of lead glass taken directly from the forming process with no further surface cutting or polishing. Extensive testing of these bars has shown that there is no measureable distinction between extruded glass and conventional ground and polished glass. The cost savings realized in omitting the surface preparation is about a factor of three. Results from our tests on extruded glass bars are given in Appendix I. They are summarized by noting that the optical properties (measured pulse heights) are identical with those for polished bars in various orientations of entering particles. The attenuation length of Cerenkov light from particles passing perpendicular to the long axis of the bar is approximately 3m. The energy resolution achieved for electrons between 2 and 6 GeV/c in an array of extruded glass is the same as that found in a conventional block of polished glass in the same beam.

The geometry of the LAPDOG calorimeters is shown in Figs. 1, 2, 3 and 4. A set of 4 central calorimeter modules surrounds the intersection point giving full azimuthal coverage and polar angle coverage down to 30° with respect to each beam. The beam's eye view (Fig. 3) shows a square cross-section for this central detector with the main ring passing through near the joint between quadrants. The individual extruded bars (typically $7 \times 7 \text{ cm}^2$ in cross-section) have their long axes perpendicular to the beam. The long axes of the bars describe lines of approximately constant θ or y (rapidity). A particle traversing the

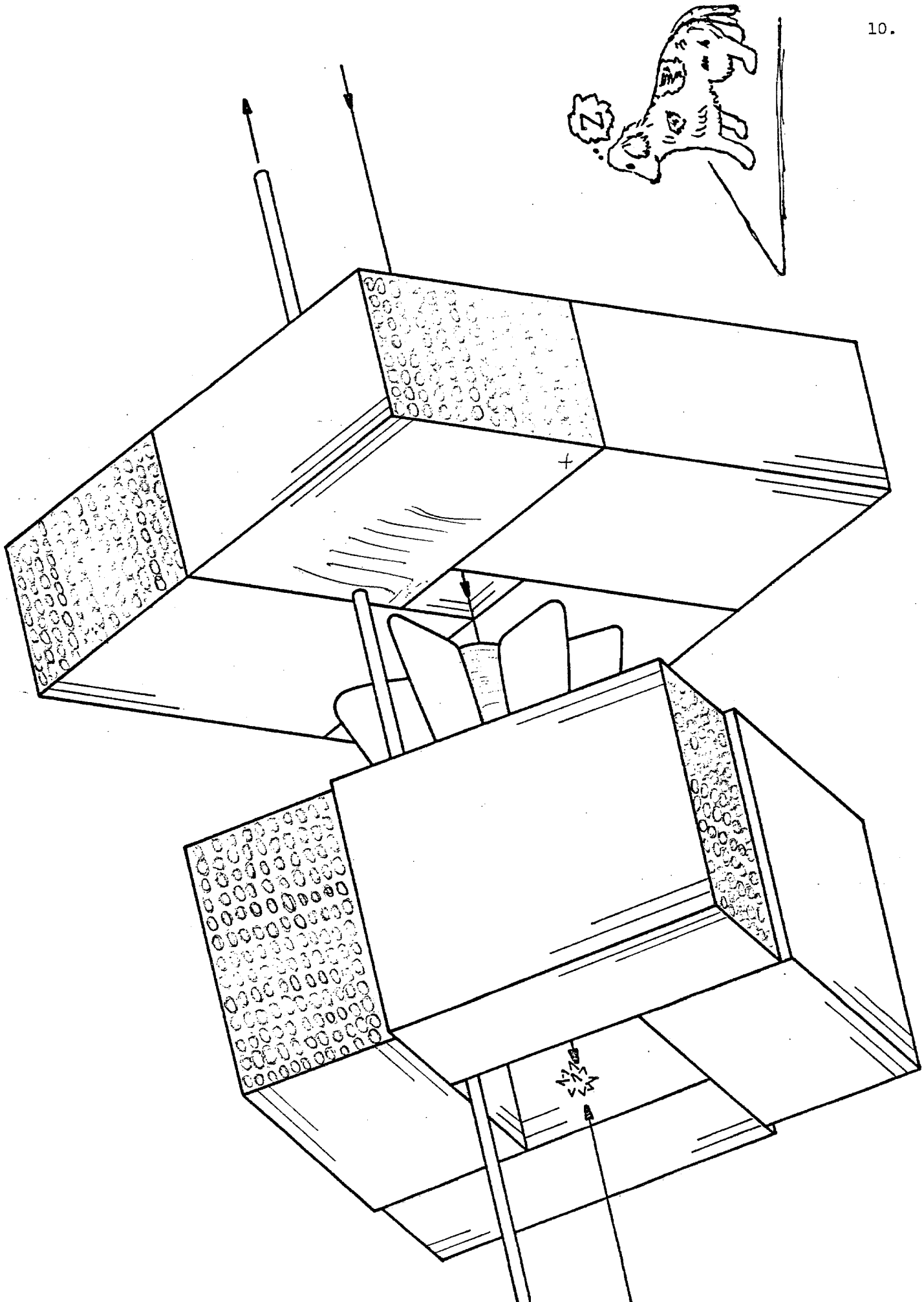


Figure 1 Schematic View of Half of the LAPDOG Detector

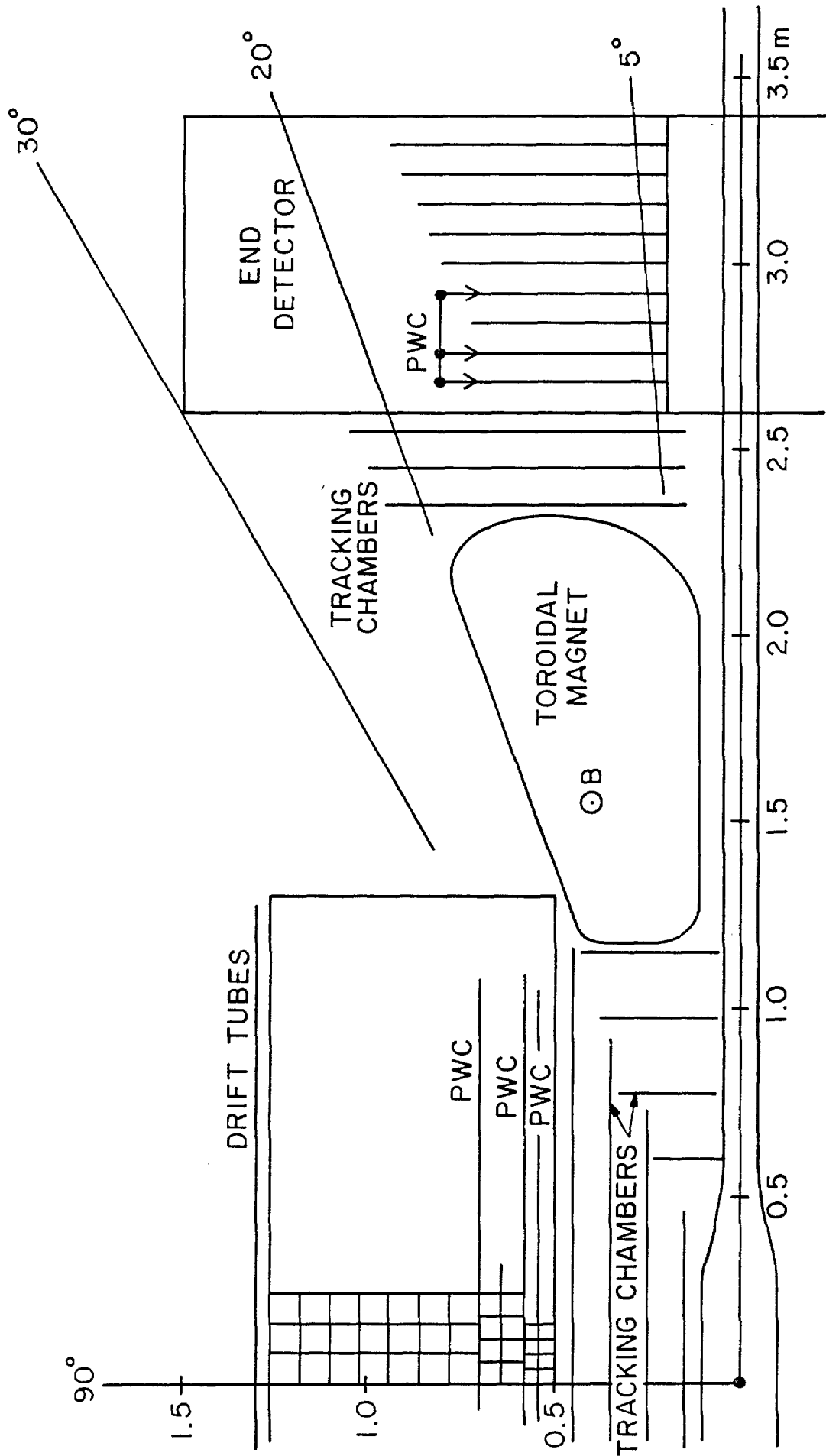


Figure 2 Polar Section of Half the Detector

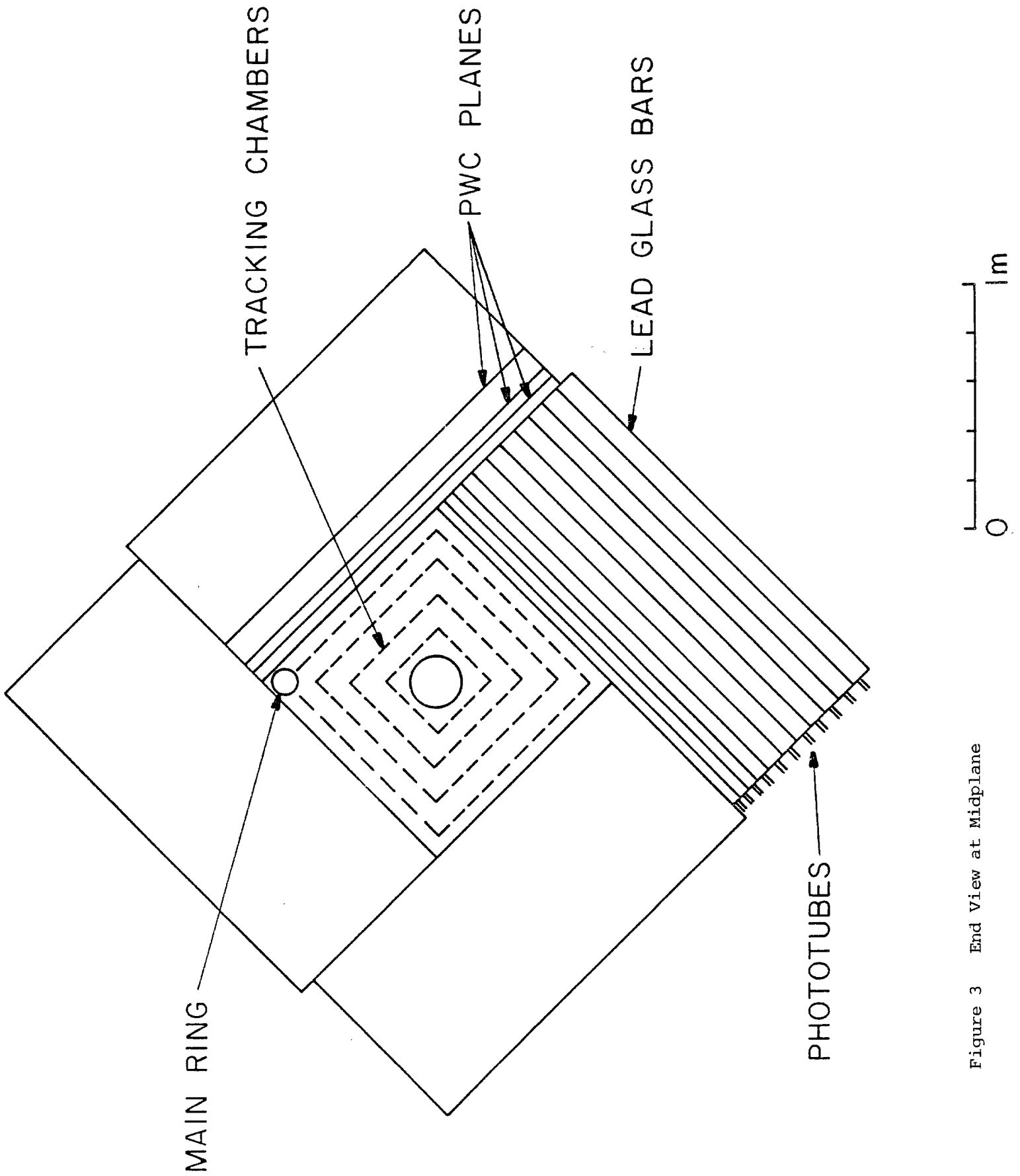


Figure 3 End View at Midplane

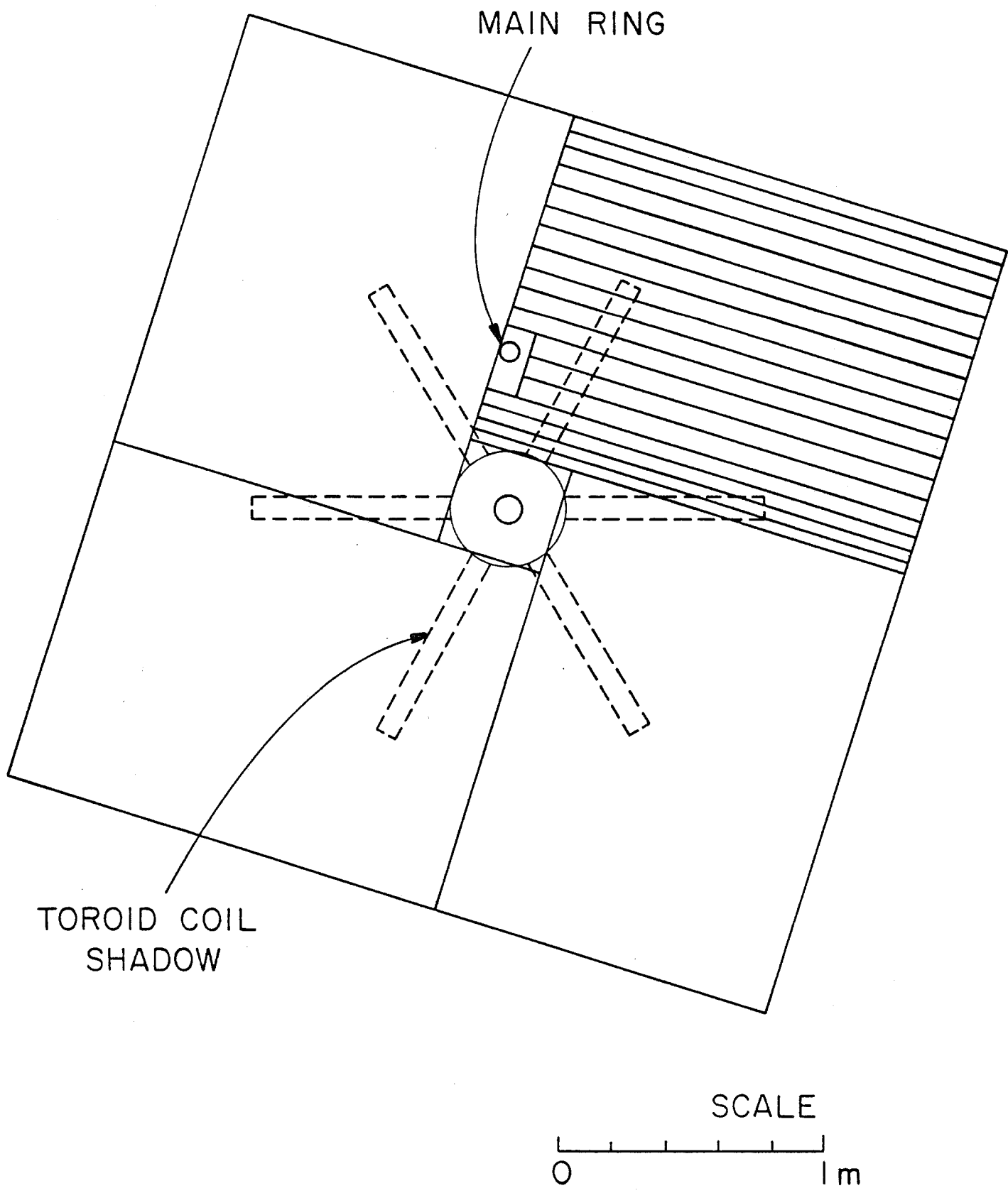


Figure 4 End View at End Detector

calorimeter from the intersection point passes through about ten layers of lead glass bars for a total thickness of 24 radiation lengths. The first two layers of bars will be of smaller thickness than the rest (~ 4 cm) whereas the last layers will be of greater thickness than average.

Each bar will be viewed from one end by a single photomultiplier of 2 inch diameter photocathode. There will be PWC planes interleaved between layers 1 and 2, 2 and 3, and between layers 4 and 5 to give both transverse coordinates of penetrating particles. The PWC planes behind layers 1 and 2 also serve to count the number of photon conversions after approximately 1 and 2 radiation lengths. This gives, on a statistical basis, the relative number of π^0 and single γ incident and forms the basis of our single photon measurement. It is similar to that of the CERN-Columbia-Oxford-Rockefeller Group at the ISR⁵ with the improvement of two samplings in compact active converters. A more detailed discussion is presented in Section IV.

The end calorimeters, in a quadrant geometry covering full azimuth between 5° and 30° with respect to the beam, are located starting at ± 2.6 m from the intersection point. The lead glass bar arrangement is similar to that for the central detector. The interleaved chambers are present here as well, with planes oriented perpendicular to the beams.

Toroidal magnets, discussed below, are situated between the central detector and the end detectors. These magnets are intended to measure the sign of particles emerging at polar angles between 5° and 20° and are primarily used for measuring the asymmetry in $W^\pm \rightarrow e^\pm \nu$ decays.

There are several important advantages to this geometry of shower detection, relative to a more conventional geometry with phototubes looking toward the incoming particles. The first is that the photocathode surface area required

for measuring the Cerenkov light is reduced. A more important advantage lies in the large number of samples of a shower obtained in its longitudinal development. Comparison of an observed shower profile versus depth with that for known electromagnetic showers greatly improves the hadron rejection power from that given by a single energy measurement. We conservatively estimate this hadron rejection to be at the level of 10^3 or more for 50 GeV particles.^{6,7} Finally, there are advantages in the geometry proposed here for energy resolution. Two of the factors influencing resolution, beyond the statistical limit imposed by photon detection, are related to lack of knowledge of the longitudinal shower profile. The first is simply the fact that some showers develop late and let some of the energy escape the detector. Fluctuations in the leakage energy add to the resolution width. The second is due to variations in the distance between shower maximum and the phototube. This fluctuation, coupled with the attenuation of light in the glass, leads to additional broadening of the resolution. This effect may also vary with time if radiation causes small changes in attenuation length. Our geometry allows us to predict, for each shower, the fraction of energy leaking out the back and to make suitable corrections on an event by event basis. Attenuation corrections can also be made since the interleaved chambers localize the shower coordinate along the long axis.

We feel that this additional power in shower energy definition should result in resolutions comparable to, or better than, that achieved in previous experiments.^{6,8-11} We recognize that a measurement of achievable resolution is crucial to this experiment and are embarked on a test in Spring '82 to determine it in a high quality electron beam. Such results, together with information on hadron

rejection, calibration and monitoring schemes, should be available for scrutiny during the review process for DO proposals.

The total requirements for lead glass bars are summarized in Table 1.

Central Detector	440 bars/quadrant	1760 bars total
	13.3 tons/quadrant	53.3 tons total
End Detectors	209 bars/quadrant	1672 bars total
	6.77 tons/quadrant	54.1 tons total
Experiment		3432 bars 107.4 tons

Table 1 Lead Glass bar count

We imagine that the calorimeters are mounted in modules; each half quadrant of the central detector and each quadrant of each end detector makes a module, or 16 modules in all. These modules also form the basic element for calibration and monitoring discussed below.

The cost of extruded glass bars in the quantity required can be estimated from advisory quotations given by Schott Optical Glass and Ohara Optical Glass, both of whom have supplied extruded bars for our tests. The price appears to be based on the total weight; we have been given the figure of \$14.35/kg. The cost for lead glass for the experiment is thus $\$1.4 \times 10^6$.

B. Tracking Chambers

This experiment does not place a premium on tracking all particles from a collision. There are however several important tasks required of the chamber systems. These are: (1) localization of electromagnetic shower in the coordinate perpendicular to the lead glass bar long axes, (2) identification of charged tracks aimed at shower deposits for electron/photon discrimination, and (3) measurement of track segments before and after the toroidal magnet in order to determine electron signs for $5^\circ \leq \theta \leq 20^\circ$. For the first two tasks, there is little premium on good spatial resolution beyond the obvious need to avoid spatial overlaps. The third task requires good resolution in order to distinguish the sign.

Locations of tracking chambers are indicated in Figs. 2 and 3. They break into several subsystems, described separately. For several of these subsystems, we adopt the chamber design used with good success by the CUSB experiment at CESR. These chambers are PWC, run at low gas gain, and with cathode plane readouts of either strip or patch variety. Anode wire signals may be read or not as desired. Position resolution, using a 0.32 cm half gap width and cathode strip width of 1 cm, is measured to be $\sigma \sim 0.5$ mm. Each channel (wire, strip, or patch) is amplified and digitized by an 8-bit ADC; the electronics cost per channel is estimated at \$32.50.

The inner chambers in the central detector region are needed to identify a charged track, if present, aiming at the calorimeter. The track density in this region is low. We plan to have 4 PWC chambers in this region, with cathode strips of 1 cm width oriented parallel to the lead glass bars. In addition,

the outermost of these chambers will have $5 \times 5 \text{ cm}^2$ patches to provide an approximate point readout at the entrance to the calorimeter.

The interleaved PWC within the calorimeter (after layers 1, 2, and 4) will be of similar construction. In this case, the coordinate perpendicular to the bar axis is obtained accurately from the pulse height division among adjacent lead glass bars (few millimeter accuracy has been reported for finely divided lead glass¹⁰). Thus we propose for these chambers to read the coordinate along the bar long axis; this is provided by Or-ing several anode wires within a 2 cm band. The last of these chambers, located near the shower maximum, will have, in addition, cathode patches of $10 \times 10 \text{ cm}^2$.

We also propose to install an array of proportional drift tubes outside the central detector to provide the hit point of a penetrating single particle. Such tracks are useful for calibration and possibly for crude muon identification. The PDT's are envisioned to be similar to the $4 \times 4 \text{ m}^2$ arrays now in use in a Brookhaven-Brown-KEK-Osaka-Pennsylvania-Stony Brook experiment at the AGS (E734). These tubes have a $3.75 \times 7.5 \text{ cm}^2$ cross-section.

The chambers in the forward region, both before and after the magnet, must have good resolution. Here we choose a small cell drift chamber system with four pairs of planes before the magnet and three pairs after. The drift coordinate is taken perpendicular to the toroidal field direction. The small size of the drift cells is chosen to achieve a suitably low multihit probability in the forward region where particle flux is high. In addition, we require for triggering and ambiguity resolution, a PWC just before the magnet and just before the calorimeter. These PWC's have wire, cathode strip and cathode patch ($5 \times 5 \text{ cm}^2$ and $10 \times 10 \text{ cm}^2$) readouts.

The PWC's interleaved within the end detector calorimeters are similar to those in the central detector.

Table 2 gives a summary of the channels required for the various subsystems. We have a total count of 13,478 channels from the PWC wires, strips and patches, and 4420 drift wires in the drift chambers and PDT's for a total of 17,898 channels. We estimate the cost for the tracking system chambers and electronics to be approximately \$1 million.

<u>Central Detector</u>		
Inside Chambers	strips	640/Quadrant = Q
	patches	828/Q
Interleaved chambers	wires (3 ch.)	240/Q
	patches (1 ch.)	352/Q
PDT's	wires (2 planes)	70/Q
Total Central Detector		8520 Channels
<u>End Detector</u>		
Driftwires before magnet		920/End = E
Patch chamber before magnet		646/E
Drift wires after magnet		990/E
Patch chamber after magnet		965/E
Interleaved chambers	strips (3 ch.)	51/Q
	patches (1 ch.)	221/Q
PDT's	wires (2 planes)	80/E
Total End Detectors		9378 Channels

Table 2 Tracking Chamber Channel Count

C. Toroidal Magnets

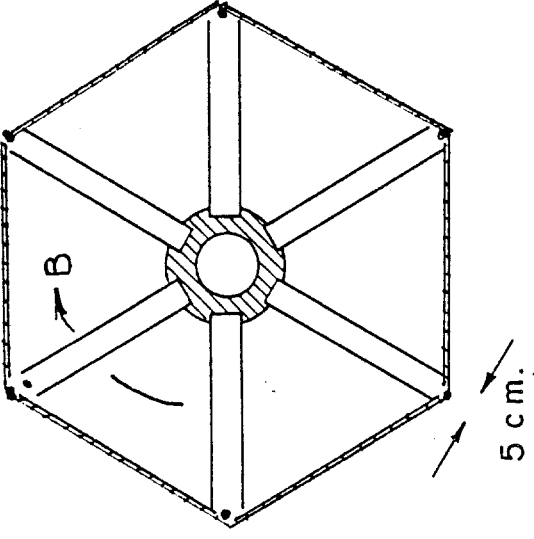
The toroidal magnets are intended to cover the polar angle region $5^\circ < \theta < 20^\circ$ and extend between 1.2m and 2.3m from the intersection point on both sides. The toroidal coils have a sextant symmetry as shown in Fig. 5; they are conventional, warm-conductor windings. Each individual coil has a thickness in the azimuthal direction of 5 cm and is wound in a spiral pattern over the whole surface of the coil plane. The properties of the toroids are given in Table 3.

The purpose of the magnets is the sign determination of electrons from W^+ decay in the kinematic regions where the correlation between beam sign and electron sign is particularly strong. This region conforms to the angular region chosen; in addition one wants to restrict the electron transverse momentum region $p_T < 35$ GeV/c where the correlation is large. A toroidal field is well matched to this problem. The field integral falls off roughly as r^{-1} , where r is the distance from the beam axis. However, at fixed p_T , the particle momentum also decreases like r^{-1} , so the magnetic deflection of particles at fixed p_T is roughly independent of angle. For $p_T = 35$ GeV/c particle, the deflection angle is about 1.3 mrad. At the chambers behind the magnet, this corresponds to a distance of 1.7 mm between the hit points for a positive and negative particle with $p_T = 35$ GeV/c. It is the need to measure this distance accurately which has dictated the drift chamber system for the forward cones.

The coils are supported by a heavy core inside 5° , as shown in Fig. 5, and by hoops outside 20° , in the region between the central and end detectors. Neither of these support structures shadows any of the detectors in the experiment. Since the position of the forward detector is determined by our choice of minimum polar angle, the lead glass cell size, and the requisite beam clearance, the insertion of the toroids does not increase the overall dimensions of the experiment. The

Forward Toroidal Magnet

END VIEW



PLAN VIEW

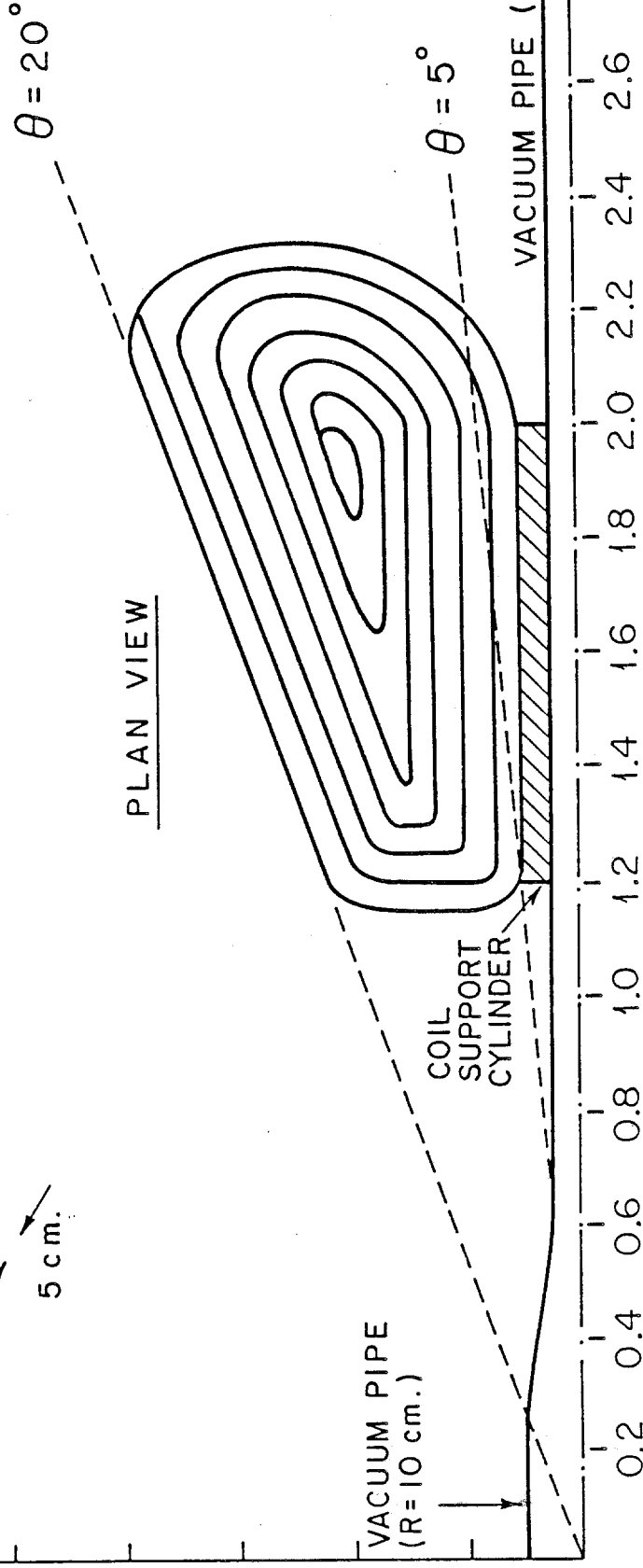


Figure 5 Toroidal Magnet

cost of each toroidal magnet is estimated at \$200K.

We note that these toroids produce no field on the intersecting beam lines, but do give a horizontal field on the main ring of about 0.4 Tm. These fields will need compensation outside our experiment if the main ring is to be accelerating protons while the toroids are on.

Number of coils	=	6 per toroid
NI	=	1.5×10^5 Ampereturns per coil
Power consumption	=	1.1 MW per toroid

Angle	Bdl (Tm)	p_T Kick (GeV/c)	Azimuthal Transparency
5°	1.8	0.54	54%
10°	0.89	0.27	77%
15°	0.59	0.18	85%
20°	0.43	0.13	89%

Table 3 Properties of the Toroidal Magnets

D. Triggering

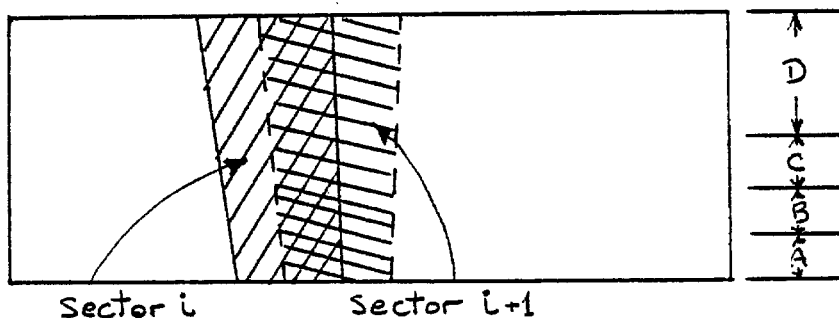
There are two important numbers to note in considering a trigger scheme for LAPDOG: The first is the time between bunch crossings ($> 2\mu\text{sec}$); the second is the mean time between beam-beam collisions at $\mathcal{L} = 2 \times 10^{29} \text{ cm}^{-2} \text{ sec}^{-1}$ ($80\mu\text{sec}$). We envision a pretrigger which makes a decision as to whether any potential beam-beam event has occurred in a time less than $2\mu\text{sec}$. If no such event is found, ADC's and clocks are reset in readiness for the next crossing. A valid beam-beam pretrigger would initiate a fast electronic analysis of the event (in about $50\mu\text{sec}$) in order to filter the events for further processing by a microcomputer or equivalent device. This filter stage must aim to reduce the rate of event candidates to 100 Hz to avoid dead time in the final stage.

We require several distinct triggers for the physics goals outlined above; obviously all triggers should run simultaneously. With their main characteristics, these are:

- 1) High mass dielectrons - There are two relatively high p_{T} electromagnetic showers with charged tracks associated. Separation of the two electrons in angle is large.
- 2) Single electrons (from W^{\pm} etc.) and single π^0 (γ) - The interesting physics here is dominantly at the largest p_{T} . Placing a cut on the p_{T} associated with a single electromagnetic shower at a high enough value will keep the single particle trigger rate low.
- 3) Low mass dielectrons (ψ, Υ) - Electrons from this category are neither high p_{T} ($\langle p_{\text{T}} \rangle$ from ψ is 1.7 GeV/c) nor large separation (minimum e^+e^-

separation in our calorimeters is about 30 cm). These represent our greatest challenge for triggering but the payoff for both physics and monitoring is large. The difficulty resides in the fact that a trigger based, say, on two electromagnetic clusters with $p_T \geq 1$ GeV/c will be satisfied by a large fraction of ordinary beam-beam events where of order ten π^0 's are produced with $\langle p_T \rangle = 0.4$ GeV/c.

For the purposes of the trigger, we will subdivide the calorimeter modules into sectors of approximately 30 lead glass bars in an overlapping pattern as shown.



Signals from each sector are summed for four longitudinal layers, A-D, and the total. Within each sector, we will obtain threshold ratio signals, e.g. if $R_A = A/\text{SUM}$, we require R_A exceed a fixed value. Such ratios R_A, \dots, R_D should be available after about 100 nsec.

Signals from the strips and patches of the interleaved chambers within the calorimeter can also be obtained relatively quickly (few hundred nanoseconds) to give information on the number of hits within a sector. Similar multiplicity information can be obtained for the strips of the inner tracking chamber.

The elements of the trigger can then be constructed as follows:

- 1) Pretrigger - A valid beam-beam event requires coincidence of the bunch crossing time signal, some energy deposit in a calorimeter sector showing a pattern of ratios appropriate to an e or γ from the intersection region, and anticoincidence of beam-gas event monitors (e.g. special beam halo counters at $\pm 5\text{m}$ from the intersection which see single beam spray 30 nsec before beam-beam secondaries).
- 2) Filter trigger - Each cluster with its sum energy exceeding some threshold and with good ratios R_A, \dots, R_D is examined. Its approximate location is found by correlating shower with interleaved PWC information. A road extending from shower center to crossing region is examined for indications of a charged particle entry. Association of shower and inner chamber hits is termed an electron candidate; absence of chamber hits yields a gamma candidate. On the basis of the information on energy deposit and hit position, a crude measure of p_T for the candidate can be obtained. The various event types desired can now be selected on the basis of electron or photon candidate multiplicity, the p_T and angular correlations among them. We envision that this stage of the trigger can be completed within tens of microseconds.
- 3) The third level of triggering occurs after ADC's have been digitized, yielding more precise energy determinations and hit positions. Computations may now be done refining the p_T and invariant pair mass calculations, with the possibility for a last stage of rejection before writing the event to tape. Other measures of interesting events

can be obtained at this stage, such as p_T imbalance, indications of jet structure, or high electron multiplicity. The nature of the hardware intended to perform this level of triggering and analysis is left deliberately vague, pending a more detailed study and advances in event processing electronics.

IV. Rates

In this section we give some details on the detection efficiency, counting rates and analysis procedures. The time interval used for all event calculations is 100 days at a luminosity of $2 \times 10^{29} \text{ cm}^{-2} \text{ sec}^{-1}$ for a total $\int \mathcal{L} dt \equiv \int_{\mathcal{L}} = 1.7 \times 10^{36} \text{ cm}^{-2}$.

The event rates computed here correspond to a detector which covers all azimuth and polar angles in the interval $7^\circ \leq \theta \leq 173^\circ$. The detector described in section III extends down to 5° with respect to the beams, but will have some small losses at detector edges and within toroid shadows.

The cross-sections for various processes have been taken for representative calculations. We have used the W^\pm and Z^0 cross-sections of Paige¹² based upon non-scaling structure functions for the hadron constituents. For $\bar{p}p$ collisions at $\sqrt{s} = 2000 \text{ GeV}$, we take $\sigma_W = 1.7 \times 10^{-32} \text{ cm}^2$ and $\sigma_Z = 1.0 \times 10^{-32} \text{ cm}^2$. Branching ratios for $e^\pm \nu$ and $e^+ e^-$ are taken as 0.083 and 0.030 respectively. The expected y (rapidity) distributions are given¹²; we assume both W and Z have invariant cross-sections which vary as $e^{-bp_T^2}$, with $\langle p_T^2 \rangle = 100 (\text{GeV}/c)^2$. The W^\pm helicity parameters are taken from Quigg¹³, which, with the V-A interaction at the decay vertex, gives the correlation discussed above between e^- and proton beam directions.

For vector ($\bar{q}q$) meson production, we use the ansatz of Gaisser et al.¹⁴:

$$B_{ee}^V \frac{d\sigma}{dx} = B_{ee}^V \frac{\Gamma_h^V}{m_V^3} f(\sqrt{\tau}) g(x) h(p_T),$$

where $\sqrt{\tau} = m/\sqrt{s}$. We take B_{ee}^ψ and B_{ee}^T to be .076 and .035 respectively; Γ_h^ψ and Γ_h^T are $5.8 \times 10^{-5} \text{ GeV}$ and $3.6 \times 10^{-5} \text{ GeV}$. The value of $f(\sqrt{\tau})$ at $\tau \rightarrow 0$ has been taken

from ISR^{3,15} data. We estimate that at Collider energies, non-scaling corrections will enhance $f(0)$ by a factor of 3 over the ISR value and thus choose $f(0) = 1.2 \times 10^{-24} \text{cm}^2 \text{GeV}^2$. The x and p_T dependences adopted from ISR data³:

$$g(x) = (1-|x|)^a$$

$$a = 3.5 \text{ for } \psi$$

$$a = 3.3 \text{ for } T$$

and

$$h(p_T) = p_T e^{-bp_T}$$

$$b = 1.7 m_{ee}^{-1/3}$$

Drell-Yan production is also taken from the ISR experimental fit³ to available data in pp collisions:

$$\frac{d^2\sigma}{d\tau dx} = \frac{A(1-\sqrt{\tau})^{10}}{\sqrt{\tau}} \frac{1}{m_{ee}^3} g(x)h(p_T),$$

where $g(x)$ and $h(p_T)$ are similar to those for vector meson production, and $A = 1.04 \times 10^{-32} \text{cm}^2 \text{GeV}^2$. We have not corrected for the difference between pp and $\bar{p}p$ at the low $\sqrt{\tau}$ values we explore.

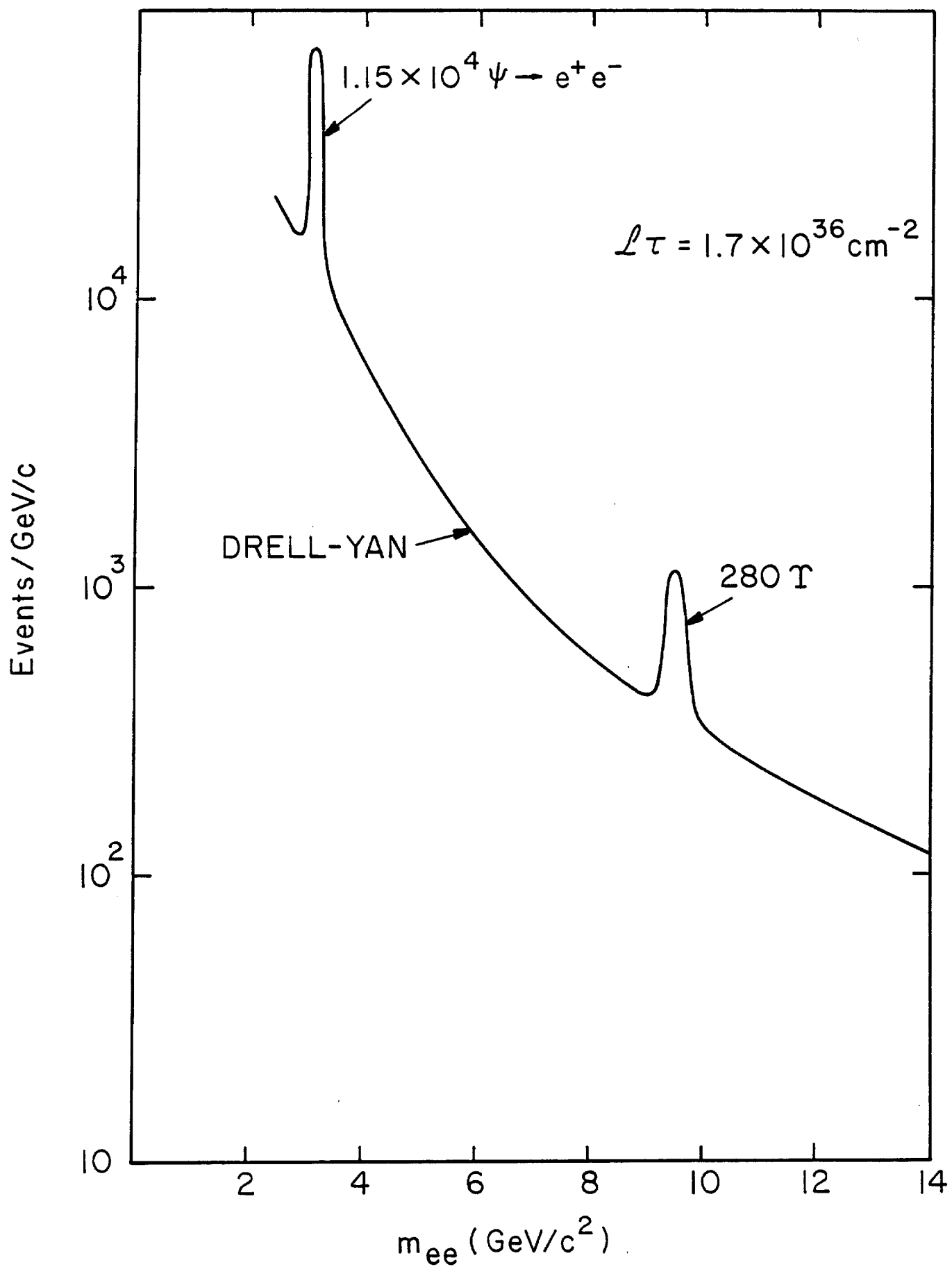
Detection efficiency for both e^+e^- at the resonances and for the continuum are given in Table 4. It is essentially uniform in p_T of the e^+e^- pair for the Z^0 ; for the lower mass states it increases by a factor of about 2 between $p_T = 0$ and $p_T = 1.5 \times m_{ee}$. The efficiency is uniform for e^+e^- pair rapidity out to $|y| \sim 2$ and falls to zero at $|y| \sim 3$.

State	Detection Efficiency
ψ	.07
T	.18
Z^0	.90
10 GeV Drell-Yan	.13
20 "	.25
30 "	.34
40 "	.45
50 "	.52

Table 4 Detection efficiency for both e^+ and e^-

Figures 6 and 7 show the number of events/GeV, dN/dm , for our total \int_L exposure and detection efficiency. Experimental resolutions have been folded in, using energy resolution for electron detection of $\sigma/E = 0.006 + 0.042/E(\text{GeV})^6$ and suitable angular errors. The ψ and T states are clearly resolved above the continuum. The Z^0 dominates the rate above 60 GeV/c². We expect $1.15 \times 10^4 \psi$, 280T, and 470 Z^0 events detected in their e^+e^- decay modes. The Drell-Yan continuum is observable out to masses of 30 GeV/c².

The relative importance of the central and end detectors varies considerably with mass for the e^+e^- pair studies. The low p_T given to an e^\pm from ψ decay causes these electrons to appear mostly in the end detectors. The ratio of e^\pm seen in the end detector to the central detector for reconstructed ψ 's is 4.6; to T it is 3.7; and for Z^0 it is about 1.

Figure 6 Detected e^+e^- Pairs vs Mass

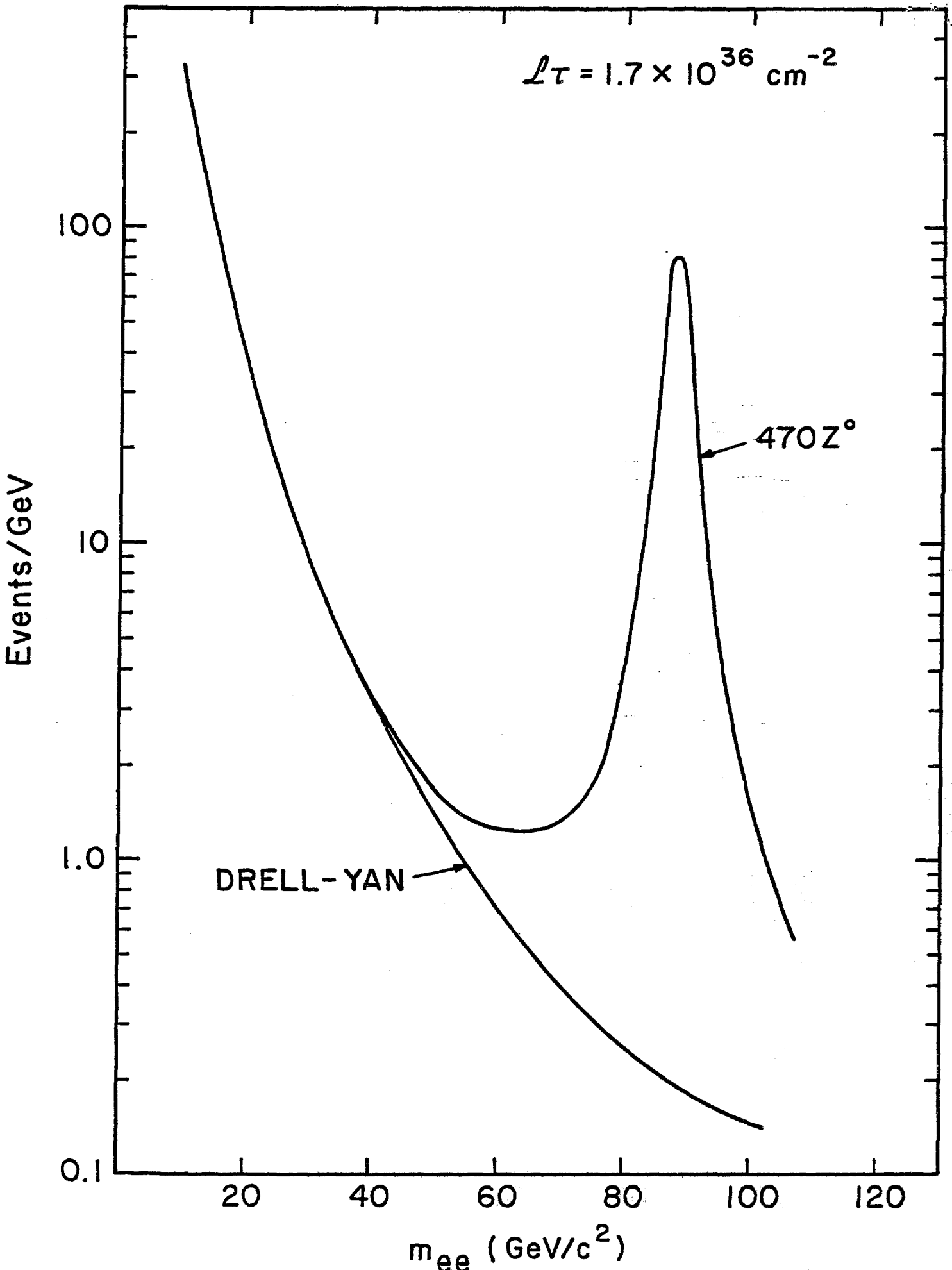


Figure 7 Detected e^+e^- Pairs vs Mass

It is clear that attaining one of the important goals of the experiment -- measuring Γ_Z for the Z^0 -- demands that the energy resolution be kept small and stable. We address the calibration and monitoring problems below in section V; here we discuss the question of how precise can a measurement of Γ_Z be.

The ideal toward which we strive is an energy resolution reported by Appel et al.⁶ of

$$\frac{\sigma}{E} = 0.006 + 0.042/\sqrt{E(\text{GeV})}$$

The constant term is believed to be controlled by systematic difficulties with calibration and stabilization. The mass resolution at the Z^0 is almost wholly determined by the energy resolution. From our Monte Carlo calculation, we find that $\sigma_m/m_Z = 0.85\%$ when electrons over the full acceptance are included with the above σ/E . If σ/E is increased by a factor 1.5 in both constant and $1/\sqrt{E}$ terms, we find $\sigma_m/m_Z = 1.21\%$.

We have generated an ensemble of Monte Carlo experiments in which a fixed $m_Z = 88$ GeV and $\Gamma_Z = 3$ GeV were used to generate a Breit-Wigner mass distribution with a fixed number of events. These events were then redistributed in mass with a Gaussian smearing function of known $\sigma_m = 0.85\%$. The resulting events were binned and presented to a fitting routine to obtain the best m_Z , Γ_Z and σ_m . The resulting ensemble averages gave the error to be expected on Γ_Z . Two ensembles were prepared: one with 1000 Z^0 events and one with 300 Z^0 events.

Our general conclusion is that the error on Γ_Z , $\delta\Gamma$, depends as expected on $N^{-1/2}$, where N is the number of events in the sample. For $N = 1000$, $\delta\Gamma = 160\text{MeV}$ and for $N = 300$, $\delta\Gamma = 280\text{MeV}$. Fits were done letting σ_m be fixed and letting σ_m

vary. A small improvement in $\delta\Gamma$ is observed if σ_m is fixed in the fit. However, we find that it is not essential to know σ_m accurately: fitting with $\sigma_m \pm 35\%$ higher or lower than that used in the Monte Carlo experiment gave the same $\delta\Gamma$. Moreover, it is not found essential that σ_m be as low as 0.85%; an ensemble prepared with $\sigma_m = 1.35\%$ yielded indistinguishable $\delta\Gamma$. Finally, we checked that the fits were independent of the choice of fitting interval. We conclude that the determination of $\frac{\Gamma}{Z}$ can be made to the desired precision if (a) the event sample used is of order 1000 and (b) the resolution function is known as a function of time. It is important that the resolution curve fall off rapidly with mass (for example a Gaussian dependence on $(m_{\text{obs}} - m_{\text{true}})$) as it is the presence of the rather wide Breit-Wigner tails which enables the fitting procedure to succeed. Little or no effect is seen on $\delta\Gamma$ if the resolution obtained in the experiment is 50% higher than our ideal. We note that in our standard luminosity interval, we expect 470 $Z^0 \rightarrow e^+e^-$ events. The Monte Carlo studies reported here suggest these will yield $\delta\Gamma = 230\text{MeV}$. Definitive exclusion of one or two additional neutrino species would require more data.

We have also calculated the single direct electron rates versus p_T for several sources. These include $W^\pm \rightarrow e^\pm \nu$, Drell-Yan and vector meson production in which only one electron is seen, and Z^0 decays with a missing e^\pm . These results are shown in Fig. 8 for our standard \int_L exposure. Also shown in Fig. 8 is the expected yield of π^0 , scaled down by a factor of 10^{-4} . The π^0 cross-section is a QCD estimate¹⁶ for $\bar{p}p$ collisions at $\sqrt{s} = 2000$ GeV. (We take the π^0 rapidity distributions to be flat out to a maximum $|y| \lesssim 3$ ¹⁶) The contribution of $10^{-4} \times \pi^0$ may be a lower estimate to the sum of direct electron production plus background from charged hadrons and π^0 Dalitz decay and conversions. Even if

dn / dp_T unpaired e^\pm
(Events / GeV/c)
 $\mathcal{L}\tau = 1.7 \times 10^{36} \text{ cm}^{-2}$

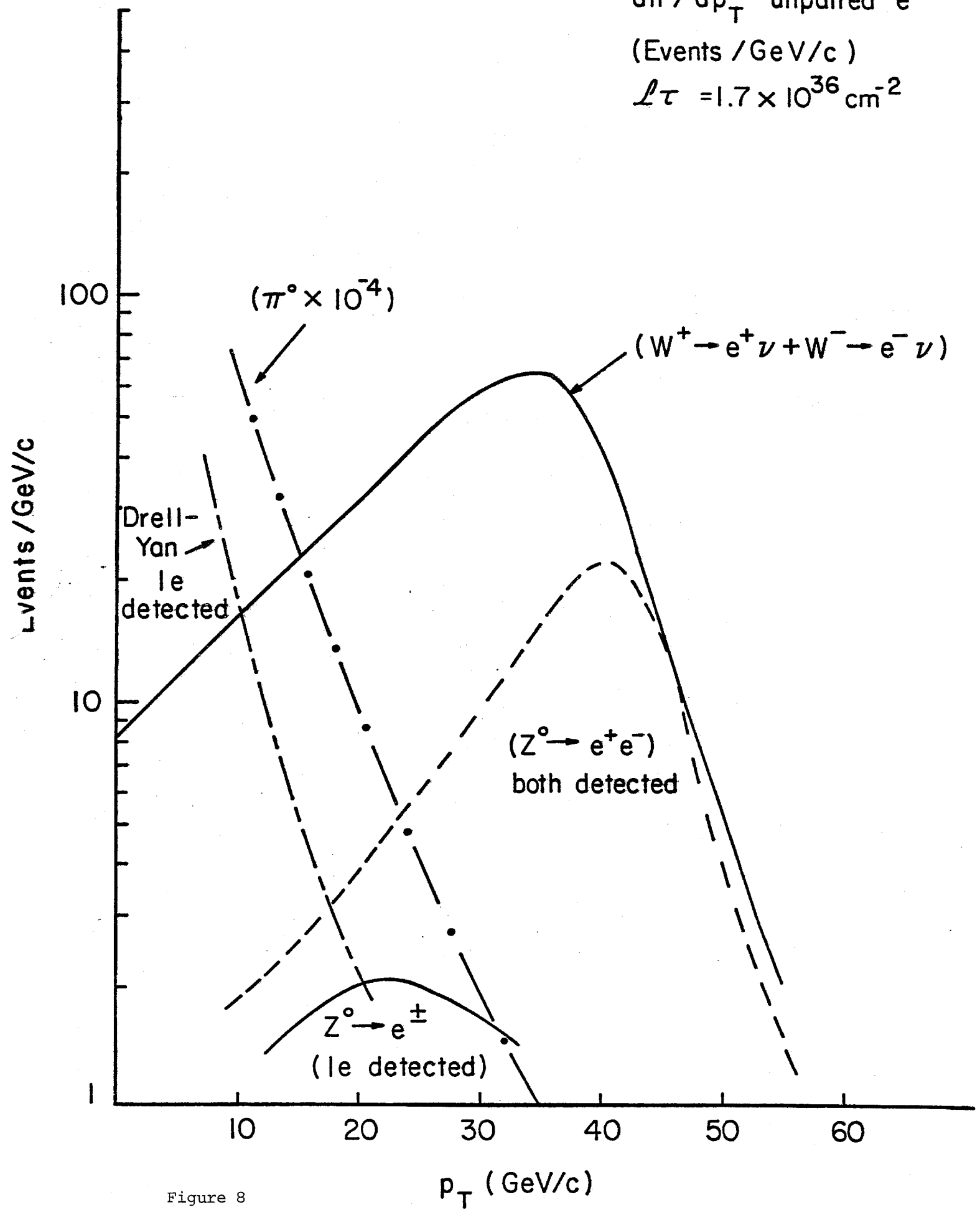


Figure 8

these sources contribute 10 times the value shown on Fig. 8, we see that $W^{\pm} \rightarrow e^{\pm} \nu$ can be observed as the dominant source of electrons above $p_T = 30$ GeV/c. We do not expect a large contamination to very high p_T single electrons from Z decays with a missing electron, since our detection efficiency for both Z^0 electrons is high.

The single π^0 yields can be read from Fig. 8. It appears that we will find inclusive π^0 production out to $p_T \sim 75$ GeV/c in our standard \int_L exposure. At a p_T value this large, it may well be that a sizeable fraction of neutral electromagnetic events are due to single photon production. We propose to measure the γ/π^0 ratio using a statistical technique similar to that employed at the ISR⁵. The two photons from a π^0 have twice the probability to show a conversion in a thin radiator as a single γ . In our case, the thin radiators are two approximately 1 r.l. layers of lead glass (a few centimeters) in the front sections of our calorimeters. The fraction of neutral showers showing conversions in either layer can be measured by both the signals in the active converter and by the PWC planes following these layers. At the ISR, a single thick, inert radiator was used and a value of $\gamma/\pi^0 \geq 0.1$ was measured. We feel therefore that LAPDOG should be capable of finding single photons if they exist at the 10% level. If a signal does exist at this level or greater, we have the possibility of detecting single photons out to $p_T = 50$ GeV/c.

V. Backgrounds

There are several backgrounds to be considered for the various aspects of this experiment. The chief among them for the e^+e^- pair portions of the experiment is the background due to an overlap between a trigger electron and some other particle. Such an overlap, if undetected, gives rise to an extra contribution to an electron's measured energy and thus shifts the apparent mass. We assert that the dominant source of extra particles near a trigger electron is the same collision that produced the high mass pair. Other, less serious, sources are beam-gas background events and unrelated beam-beam events.

We rule out beam-gas collisions as a dominant source of backgrounds partly on the basis of experience at the ISR. There, at luminosities of order 10^{29} $\text{cm}^{-2}\text{sec}^{-1}$, beam gas backgrounds are typically less than or equal to beam-beam rates. At the Collider, this luminosity is achieved by lower currents and smaller beam heights than at the ISR. Since beam-gas collisions scale with the currents in the beams, we expect the beam-gas events will be suppressed in Collider operation. Considerable further suppression is afforded by our ability to determine a vertex to within 1mm along the beam directions, using the inner chamber system.

Backgrounds from beam-beam collisions other than the one of interest are also small for average luminosities of 2×10^{29} $\text{cm}^{-2}\text{sec}^{-1}$. Mean times between beam-beam collisions of any sort ($\sigma \sim 60$ mb) are about 80 μ sec. The beam bucket crossing interval is at most 7 μ sec, so the average number of interactions per crossing is less than 0.1. Instances in which two interactions occur can be

readily identified using the information on the vertex coordinate along the beam. In any case, the superposition of a second event upon the first happens less than 10% of the time.

In order to estimate the probability for an extra track to overlap with an electron (or photon) of interest, we have studied Monte Carlo simulations²¹ of $\sqrt{s} = 2000$ GeV collisions. We have generated a number of "minimum bias" events in which diffractive interactions result in the production of 25 charged particles on average and a comparable number of stable neutrals (γ 's, K_L 's, n's). These particles give a central rapidity plateau of about 1.5 charged particles per unit of rapidity (and thus most particles at small angles). We have let these particles hit our simulated detector and determined both the average multiplicity in each counter and the average energy deposit.

For the central detector, we find the average number of charged particle hits per cell of the calorimeter is about .03 per event. Defining an area of overlap, within which a second hit might not be resolved, to be 2×2 cm², we find that there is a 1×10^{-4} probability for there to be a second charged particle in the vicinity of a trigger electron. The overlap of photons is about a factor of 10 worse due to the somewhat poorer two-cluster resolution in the calorimeter. Even allowing for considerable fluctuation in particle densities, we find that overlaps in the central detector are a small problem. The situation in the outer portions of the end detectors is of similar magnitude.

The most serious potential problem for extra hits and energy deposits obviously arises in the smallest angle region of the end detectors. Figure 9 shows the multi-hit probability (charged plus neutral) in each lead glass bar of

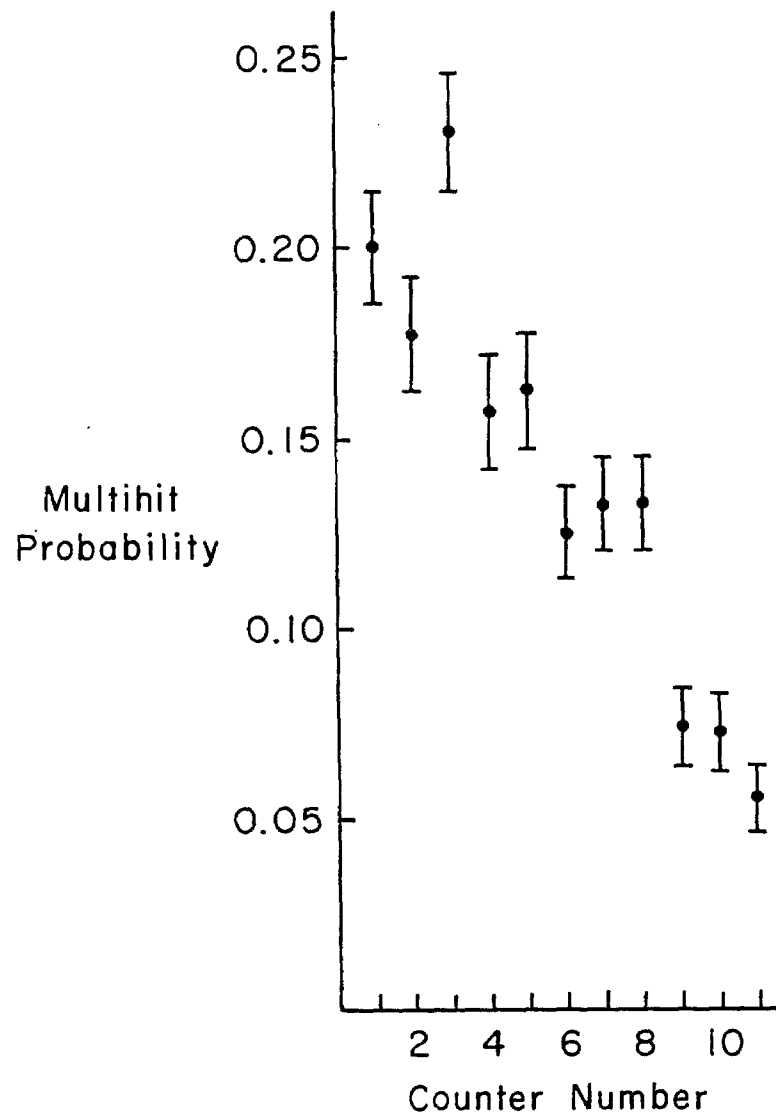


Figure 9 Multi-Hit Probability in End Detector Counters

the end detector. Cells are numbered with #1 closest to the beam line and correspond to the geometry of Fig. 4; the cell (bar) widths are 4cm for the first two, 6cm for the second two and 8cm thereafter. We see that the multiple hit probability decreases from about 0.2 near the beams to below 0.05 (per interaction) beyond cell 10.

Figure 10 shows the distribution of particle hits (per beam-beam collision) versus radial distance from the beams at one of the end detectors. The units are hits per 4cm increment in distance (the smallest of our lead glass bar widths is 4cm and the largest is 8cm). Also shown in Fig. 10 is the distribution in energy carried by particles versus distance from the beams. We find that at the smallest distance from the beam (20cm), the average energy carried by charged particles is 3.8 GeV and the average carried by neutral particles is 2.0 GeV. The worst case for an excess undetected energy deposit in a counter struck by a trigger electron is a photon hitting within 6cm of the electron (probability $\sim 5 \times 10^{-2}$) carrying mean energy of 2 GeV. The average energy of an electron from a Z^0 at this angle is over 200 GeV. Thus even at the smallest angle, the effect of these random overlaps is that 1 in 20 Z^0 events contains an electron with an added energy contribution of the order of 1%. Further studies of these backgrounds are in progress. In any case, the data themselves will provide the appropriate distributions of unwanted particle hit locations and energy deposits to allow these effects to be monitored and subtracted.

For the single particle measurements at high p_T , a similar problem of overlap may exist. It will cause a deviation of the measured p_T from the true p_T by a small amount in a small fraction of the events. High p_T π^0 (or photon) candidates

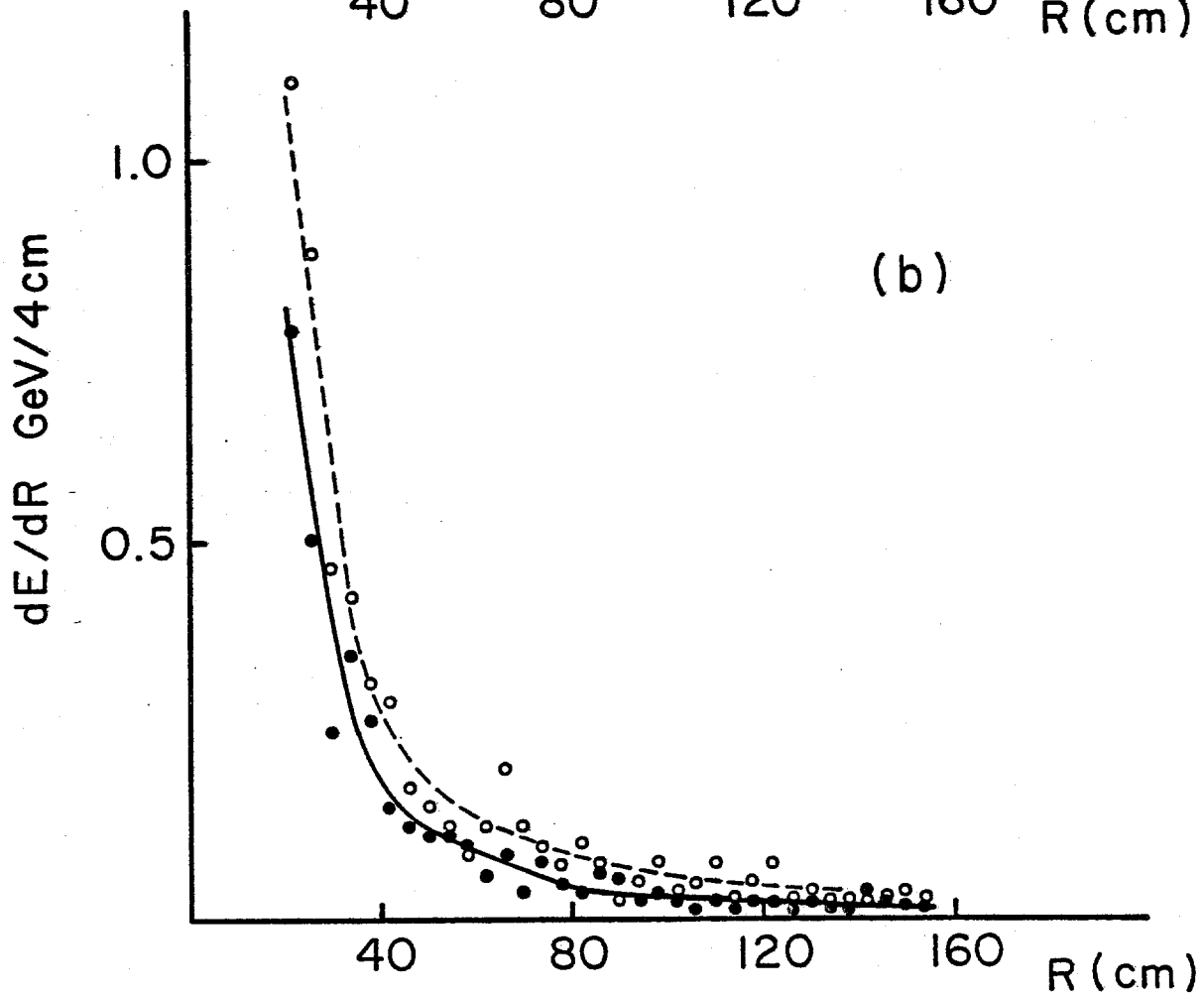
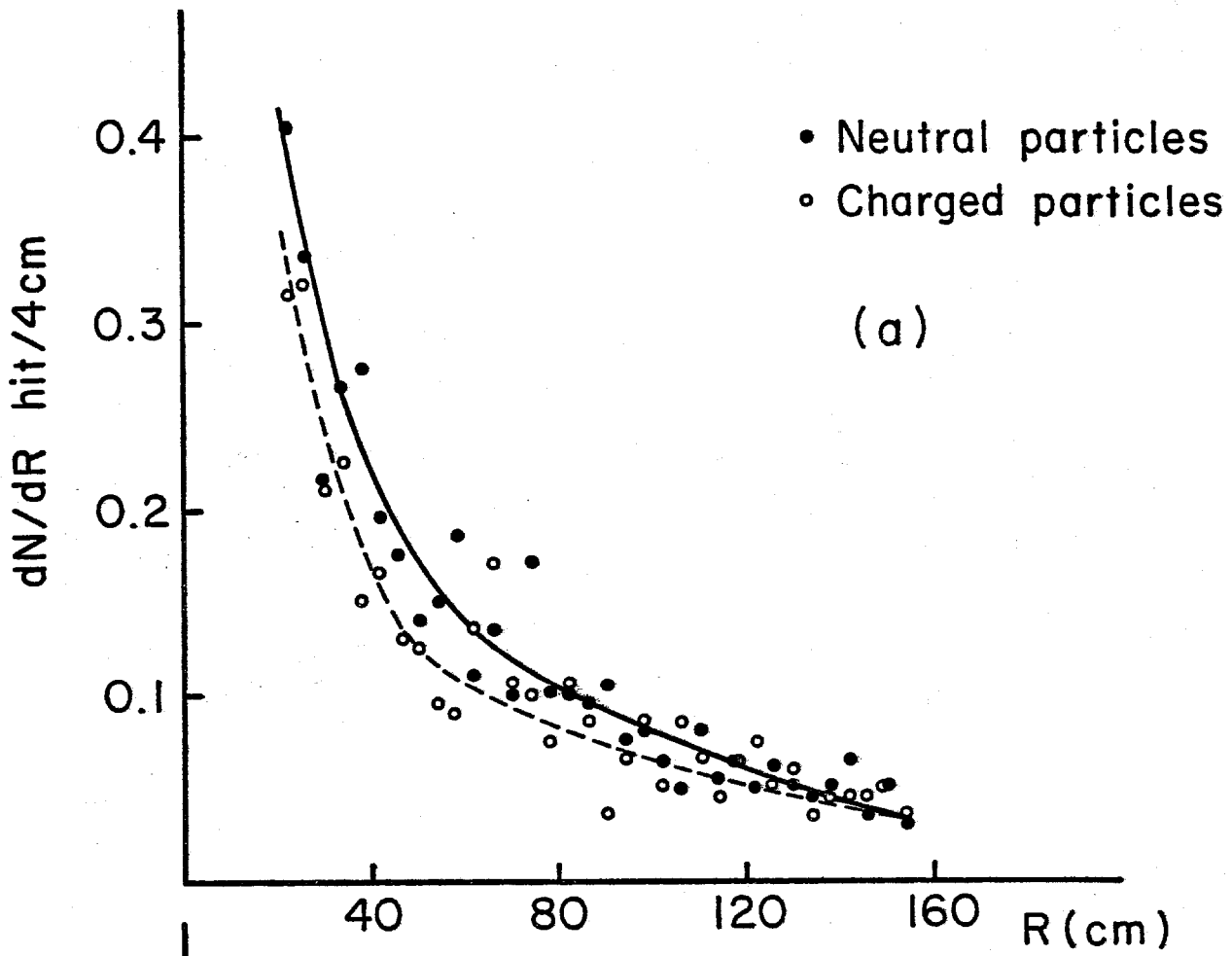


Figure 10 (a) Radial Hit Distribution; (b) Energy Distribution in End Detectors

will occasionally be lost due to overlap with a charged track. Neither of these effects seem to be likely to cause significant distortions of the measured spectra. A more serious difficulty is the misidentification of a charged hadron as an electron. This effect, discussed above in section IV is estimated to overwhelm single electron measurements below 30 GeV/c. Above this value, in the region populated by w^{\pm} decays, the above sources of background appear to be manageable.

VI. Calibration, Operation and Monitoring of Lead Glass

As discussed above, we require an energy resolution of σ/E of about 1.5% at $E = 100$ GeV (the typical electron energy from Z^0 decay), with a stability of similar magnitude in order to make a definitive measurement of the Z^0 width.

While this is close to the state-of-the-art in the use of lead glass, it is less important to achieve the ultimate resolution than it is to have it stable and its value known. Several groups have achieved 1.5% resolution in actual experimental conditions.^{8,9,10,17} Our preliminary tests with lead glass and recent developments in stabilizing monitor systems¹⁸ make us confident that we will be able to do at least as well. However, to confirm this expectation we are making a test of a substantial lead glass array with tagged electrons and a preliminary monitoring system in a beam at Fermilab. These results will guide us in our final choices.

Although there will no doubt be modifications to our calibration, operating, and monitoring scheme as described below, we believe it will prove to be adequate to achieve our technical goals. Pending the results of our test, we would proceed as follows:

- 1) The sixteen modules of lead glass will each be assembled in complete, self-contained units. Eight of them for the central detector contain 220 blocks and tubes each and eight for the end detectors contain 209 blocks and tubes each. This is a convenient size from a system and handling point of view. Included in the assembly will be a fiber optics harness which couples a filtered light source to each phototube in the module (at this time a high intensity¹⁹ LED, stabilized to $< 0.25\%$, is planned, pending further investigation of laser sources). Each module will have its own microprocessor which will handle the

the readout and control, and will check the calibration systems. The light system is in turn monitored by "master", redundant phototube monitors which have independent Americium-241 source, cosmic ray, and light references. The individual modules will have $\pm 1^\circ\text{C}$ temperature controls. We intend to have H.V. compensation for the phototubes but the PIN photodiode stabilized sources have a $0.025\%/^\circ\text{C}$ coefficient¹⁸ so this degree of temperature control will be more than sufficient.

2) After complete assembly and temperature stabilization of each module, phototube responses will first be roughly equalized using the light pulser and "vertical" cosmic rays. By "vertical" cosmic rays we mean that the module is oriented with the blocks' long dimension vertical, with the phototube end at the bottom. In this orientation, up to 2 GeV is deposited in each block. Small, computer driven potentiometers at the end of each dynode chain permit individual phototube response equalization. Experience gained in the AGS experiment E-734²⁰ in matching 4000 tubes and also the experience of "GAMS 200"¹⁰ and "GAMS 4000" show this to be straightforward.

3) Next, each completed and self-contained module is moved into a test beam capable of delivering about 400 tagged electrons per burst. The module is mounted in a test rack such that it can be rotated about an axis perpendicular to the long dimension of the block. This permits orientation of the blocks with the beam at arbitrary angles. Beam muons would be used along the block axis as a check on "vertical" cosmic rays - this is readily and quickly done with the beam defocused sufficiently to cover about 10 blocks simultaneously. Next under similar defocus conditions, the module is rotated to its "standard" position

(beam perpendicular to the long dimension of block) and exposed until a sample of ~ 3000 momentum analyzed electrons per entrance block have been accumulated. This should take about 5 hours. A conventional matrix technique is then used to extract the calibration constants, α_j , via minimizing a quantity

$$X = \sum_{i,j} (\sum_j \alpha_j P_{ij} - E)^2$$

where j is the block index and i is the event index. One end module and one central module are calibrated at several energies to obtain the parameters versus energy. Light pulser monitor data are taken interspersed with the above mentioned tests and permanent files are created. Each of these modules would be cycled through these tests twice, the tests to be separated by the 16' module cycle time. The individual modules would be kept under their own environmental control and light source (together with cosmic ray) monitoring for stability; thus a check on the monitor system will be made. The same test beam calibration procedure is to be repeated after the physics run. We estimate 200 hours of test beam time will be necessary, both before and after the main run.

4) Additional checks must be made on pedestals and the analogue and digital portions of the electronics for each channel. We plan to achieve this by the use of a calibrated filter set in the light pulser system which allows us to detect non-linearities, and by the use of an electronic pulser which can inject a calibrated amount of charge into each channel in a computer-selectable way. This will make a direct check of electronic linearity and digitization. Again E-734 and CUSB are existence proofs for the feasibility

and simplicity of monitoring a large system; several of us are involved in these experiments.

5) The modules and their integrated calibration systems will then be installed on their carriers in the DO area. A master light distribution system with phototube monitors - identical to the individual module light distribution systems - will be installed. This master is intended to monitor the relative stability of the individual module systems.

With a luminosity of $2 \times 10^{29} \text{ cm}^{-2} \text{ sec}^{-1}$ the opportunities for calibration from beam related calibration reactions are limited. However one does not have to rely entirely on the stability control of the pulser and monitor system, because for the eight modules which form the end detectors there is an appreciable $T \rightarrow e^+e^-$ signal (with average electron energy of 24 GeV) and a strong $\psi \rightarrow e^+e^-$ signal (with average energy of 9 GeV). In a run of 100 days, there would be about 200T and 8000 ψ events in the end detectors. Because of the negligible intrinsic widths of the T and ψ , these events determine the resolution function and mass scale independently for these 8 modules. They also give indirectly a measure of the effectiveness and sensitivity of the monitor system and give confidence for the integrity of the remainder of the glass exposed to lower rate.

Although this outline of our intended procedures is necessarily broad for such a document as this, it is based in scale and precision upon proven techniques with little or no extrapolation. The orientation of the blocks is somewhat novel and the glass finish is different. However, we believe the tests we have performed so far combined with the current tests will substantiate the technique.

VII Summary

The LAPDOG proposal is focussed on high resolution studies of electrons and photons produced in $\bar{p}p$ collisions. The primary detection system is a finely divided array of low-cost extruded lead glass bars.

The detector itself occupies a space $\pm 3.5\text{m}$ along the beams and $\pm 1.5\text{m}$ transverse to the beams. The hall dimensions required to house the experiment should be at least $5\text{m} \times 5\text{m} \times 9\text{m}$.

Two toroidal magnets consume 2.2MW of power; no cryogenics are required. These magnets, when powered, give field integrals of about 0.4 Tm along the main ring beam line for each magnet. If injection is to take place while these magnets are on, a compensation scheme must be implemented.

The calorimeters will be mounted in separate modules; crane capacity of 20 tons will be sufficient to load these modules into place. We foresee the need for a staging area above or beside the DO hall, of dimensions approximately $10 \times 10 \times 10 \text{ m}^3$, in order to assemble the experiment and to withdraw it during fixed target operations.

The main costs for construction of LAPDOG are summarized in Table 5.

Calorimeter	
Lead Glass (3432 bars)	\$1.4M
Phototubes/cabling	0.4M
ADC	<u>0.2M</u>
	2.0M
Track chambers (13,478 PWC and 4420 Drift) including chamber construction	1.0M
Toroid Magnets	0.5M
Calibration Systems (fiber optics, light sources etc.)	0.3M
Data Acquisition/Computer	0.5M
Mechanical Supports	0.5M
Total	4.8M

Table 5 Cost Summary

Our proposal is based on a requested luminosity integral for $\bar{p}p$ collisions of 100 days at $\mathcal{L} = 2 \times 10^{29} \text{cm}^{-2} \text{sec}^{-1}$, or $\int \mathcal{L} dt = 1.7 \times 10^{36} \text{cm}^{-2}$. In addition, we require time in a test beam capable of delivering about 400 momentum analyzed electrons per burst. We estimate a total test beam time of 200 hours will be required for calibration of the calorimeters, both before and after our run.

Appendix I - Tests of Extruded Lead Glass Bars

Lead glass has been used in many high energy experiments where good energy resolution is required for photons and electrons. The advantages of lead glass are its small radiation length, transparency, and the fact that electromagnetic showers are fully visible. The major disadvantage is its cost, which is in the vicinity of \$40/kg. Many geometric arrangements have been used, but the most standard has been an array of blocks (typically 15 x 15 cm² in cross-section) viewed by a photomultiplier facing the incoming particles. Several experiments have used one or two thinner layers preceding the large blocks with photomultipliers viewing these layers from the edges; energy resolutions in these hybrid arrays has typically been as good as the single blocks viewed from the end.

Over the past year, we have pursued a program of testing lead glass bars taken directly from the extrusion or extrusion casting process employed by the glass manufacturers. Such bars are routinely produced as blanks with cross-sections varying between 3.5 x 3.5 cm² to 8 x 8 cm², in lengths up to 180 cm. The surfaces of these bars are rippled, with wavelength of several millimeters and amplitudes of a few tenths of millimeters. However, the small scale surface quality is excellent and they appear to be optically as smooth as any polished glass.

Working with two glass manufacturers, Schott Optical Glass (USA) and Ohara Optical Glass (Japan), we have found that some further economies in lead glass production can be made and that high optical quality bars with few inclusions or surface scratches can be produced in quantity for prices below \$15/kg.

We have tested the optical properties of extruded bars from Schott and Ohara and compared them with a polished bar from Schott made from the same ingot as the polished bar. The number of photons, and response versus angle and distance from photomultiplier, were indistinguishable from polished glass when tested with Cerenkov light from a muon beam. These optical comparisons are shown in Appendix II.

Figure I-1 shows a 140 cm long bar of F2 glass, similar to that proposed for LAPDOG. This bar was mounted with a mirror on the end opposite to the phototube and exposed to muons traversing the bar perpendicular to its long axis. Figure I-2 shows the pulse area measured with an S-20 photocathode, versus distance from the photomultiplier. The straight through muons deposited 50 MeV of energy. The attenuation curve shows a sharp drop over the first 10 cm, corresponding to the rapid attenuation of short wavelength light. Beyond 10 cm, the attenuation length becomes long -- the order of 3m over the remainder of the bar. Recently, there has been a report¹¹ of further flattening of the attenuation curve by interposition of a filter between glass and phototube, such that pulse areas vary by less than 2% over the length of a 60 cm long polished bar. We will continue to investigate the optimization of attenuation length and measured light intensity through matching of lead glass type, filters, mirrors and phototube response.

We have investigated the response of an array of extruded lead glass bars to an electron beam at Brookhaven in the energy range 2 to 6 GeV. This array was a 3 block (perpendicular to the beam) by 10 block (along the beam) stack using $6.5 \times 6.5 \times 60 \text{ cm}^3$ bars, shown in Fig. I-3. The beam was of poor quality, having a $\delta p/p$ spread for hadrons of $\pm 3\%$, determined from the Cerenkov threshold



Figure I-1 65 cm and 140 cm F2 Extruded Bars

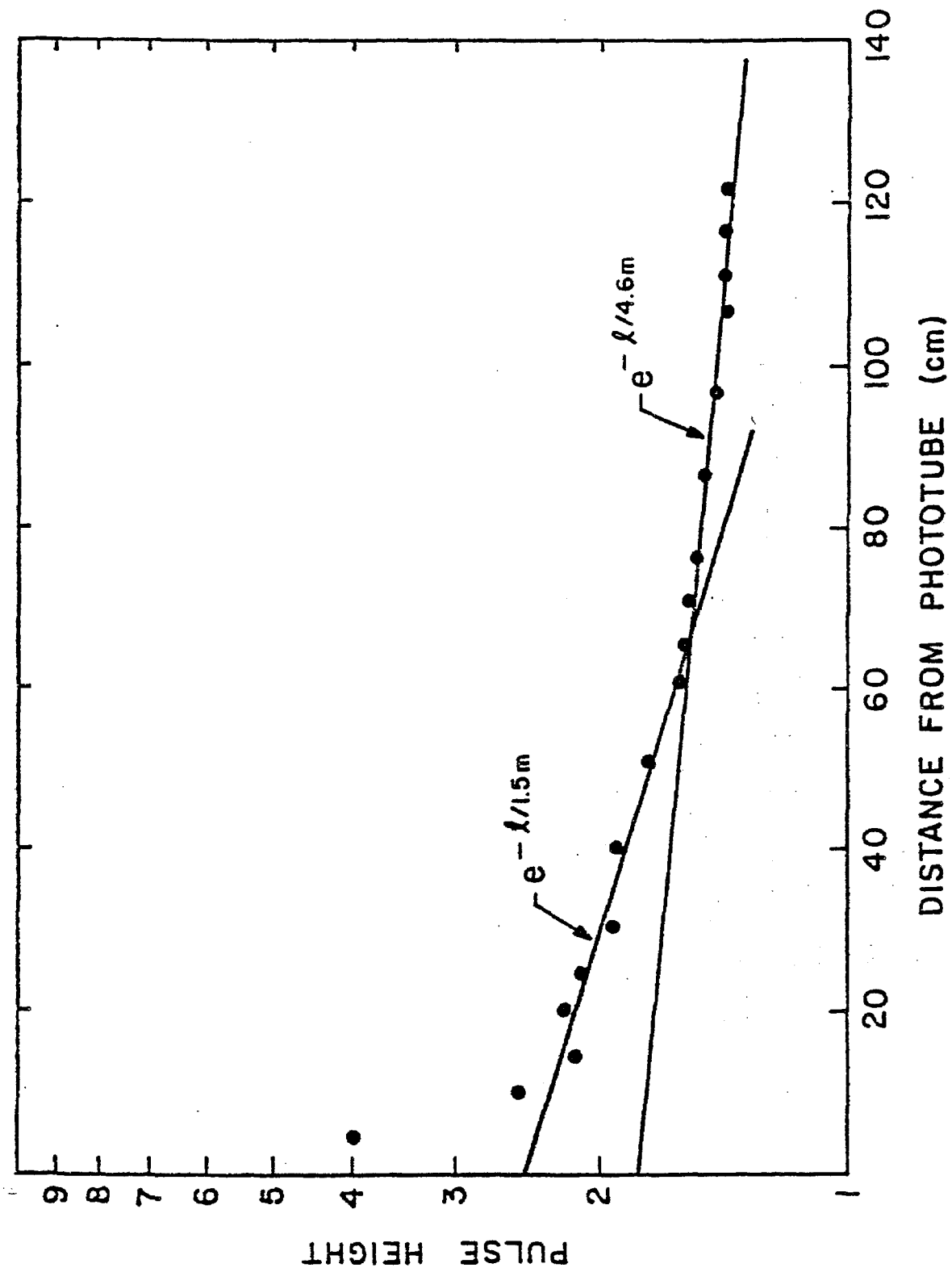


Figure I-2 Attenuation Curve



Figure I-3 . 30 Bar Test Array

curve. (The electron momentum definition was worse, owing to scattering and bremsstrahlung in various materials in the beam line.) Figure I-4 shows the energy distribution in a 4 GeV run, with hadrons partially suppressed by a Cerenkov requirement. In addition to the hadron contamination, we observe an excess of events in the electron peak on the low energy side due to bremsstrahlung. Figure I-5 shows the effect on this sample of the simplest hadron rejection cut; this was the requirement that more than half the observed energy be recorded in the first three layers (~ 6 r.l.). The electron signal is unaffected whereas the hadron peak is reduced by a large factor. Clearly a more refined algorithm based upon the longitudinal profile expected for electromagnetic showers will enhance hadron rejection. Figure I-6 shows the effect of a cut designed to remove bremsstrahlung events from the sample of Fig. I-5. This requirement demanded low pulse areas in the front layer bars above and below the beam impact point. We observe that the low energy tail of the electron peak has been essentially removed. We feel that these rather simple cuts demonstrate the power available in such a highly modular array as proposed for LAPDOG - both in hadron rejection and in tagging multiple electromagnetic particle hits.

Figure I-7 shows the mean energy deposit versus depth for 4 GeV electron showers. This curve shows the well-known longitudinal distribution with a maximum around 4 r.l. We observe the logarithmic increase of the depth at showers maximum with energy. One of the strong advantages of our multilayer array is the possibility for predicting the fraction of energy in any given shower leaking past a certain depth. If this fraction can be predicted for a shower, based upon the observed profile in earlier layers, it becomes possible to achieve good energy resolution in a thinner array of lead glass.

ENERGY DISTRIBUTION

NO CUTS

4 GeV BEAM

EVENTS

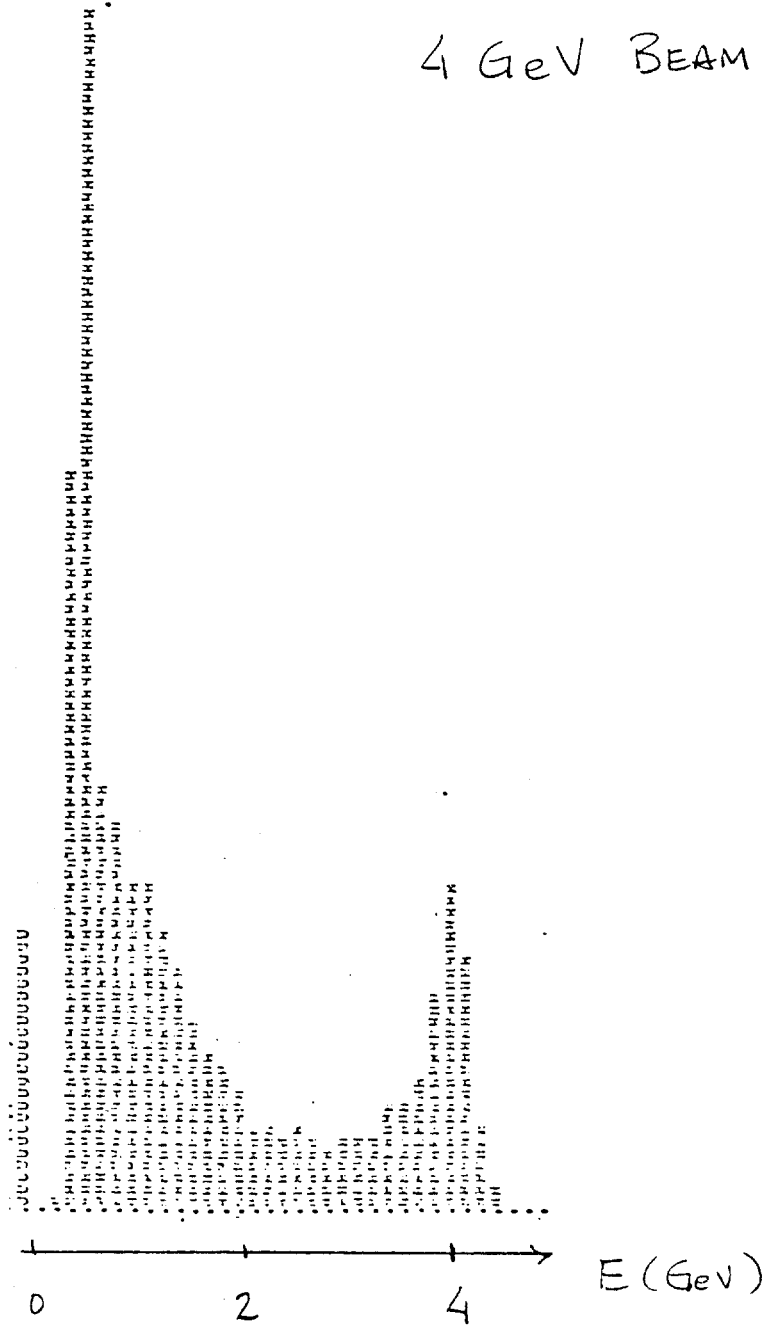


Figure I-4 Raw Energy Distribution

BEAM →

2	0	39	42	0	0	0	0	0	0
42	40	225	236	37	76	74	37	55	17
0	0	1	0	41	26	33	0	1	5

$\Sigma E = 1035 \text{ MeV}$

TYPICAL EVENT REMOVED
BY "HADRON" CUT

56.

ENERGY DISTRIBUTION

CUT ON RATIO OF
ENERGY IN 1ST
6 RADIATION LENGTHS

4 GeV BEAM

EVENTS

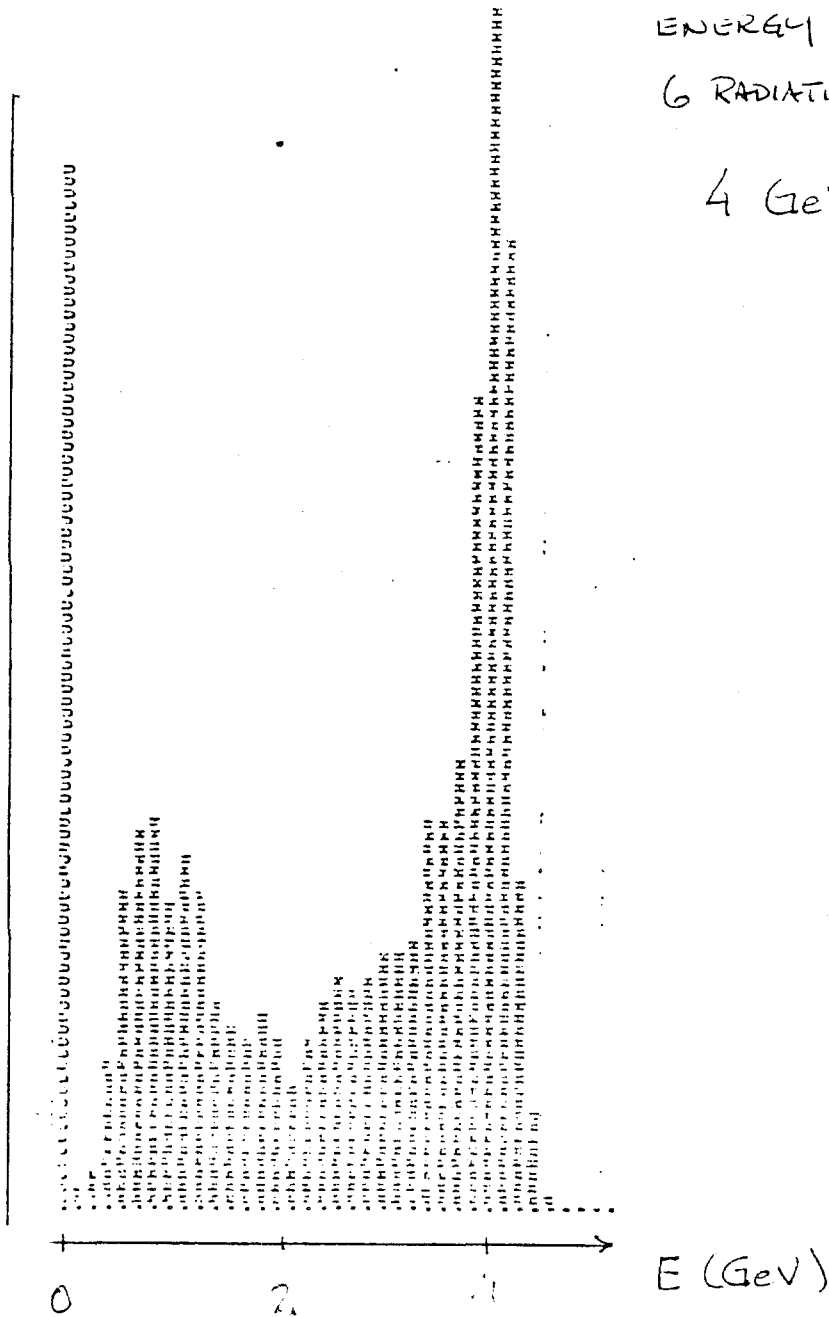


Figure I-5 Energy Distribution after Hadron Cut

TYPICAL EVENT REMOVED
BY "BREMSSTRAHLUNG" CUT

BLAM →

62	84	15	45	4	1	1	0	5	3
329	1225	302	377	155	29	13	7	4	2
4	20	37	25	19	30	12	7	2	0

57.

$$\sum E = 2940 \text{ MeV}$$

ENERGY DISTRIBUTION

CUTS ON CORNERS
(BREMSSTRAHLUNG)

AND RATIO (HADRONS)

EVENTS

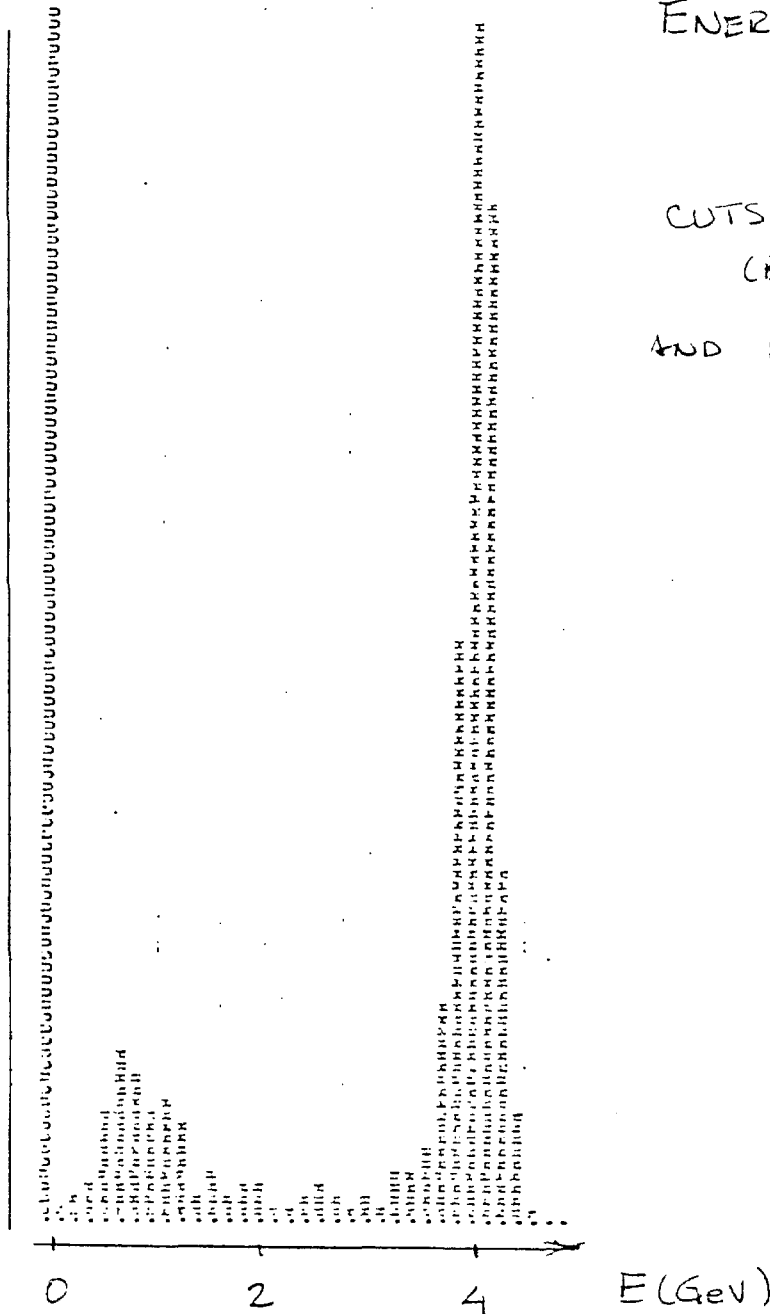


Figure I-6 Energy Distribution after Bremsstrahlung and Hadron Cuts

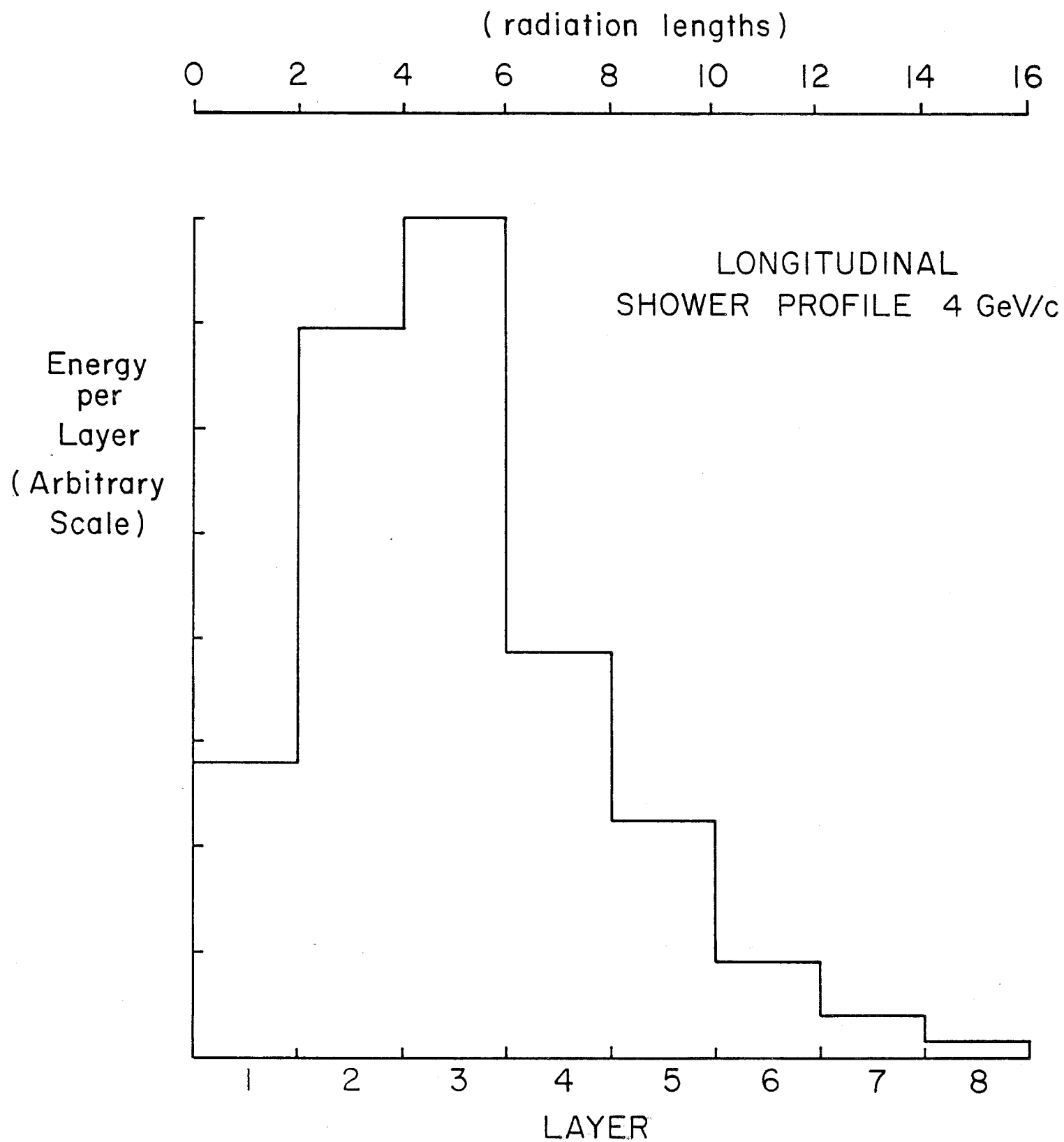


Figure I-7 Mean Longitudinal Shower Profile

We have examined this possibility with our test array data. For a particular run, we ignored the bars comprising layers 7 to 10 (from 12 to 20 radiation lengths). The energy distribution seen in the preceding layers was fitted to a universal shower curve for each event, and a prediction made for the energy that would have been seen beyond 12 radiation lengths. Figure I-8 shows the energy distribution actually observed and also the distribution obtained using the sum of the observed energy in the first 12 radiation lengths plus the predicted energy thereafter. The two distributions agree. In this particular case, the average energy added for the shower beyond 12 radiation lengths was about 3%, with large fluctuations.

We have fitted the gain constants, α_j , for the 30 bar array to achieve the best electron energy resolution by minimizing the quantity

$$X = \sum_i (\sum_j \alpha_j P_{ij} - E)^2,$$

where P_{ij} is the observed pulse areas in the i th event. The starting point for this minimization was the set of constants obtained from straight through muon calibration. We have compared the resolutions obtained with that found using a single lead glass block (15 x 15 x 35 cm³). The array resolution is comparable to that for the single block. Figure I-9 shows the resolution achieved at several energies; some variation is observed, in part due to changing beam conditions. The observed resolutions are compatible with $\sigma/E = 0.08/\sqrt{E(\text{GeV})}$. The measured $\delta p/p$ for hadrons in this beam are sufficient to account for about half of the observed resolution.

4 GeV ELECTRONS

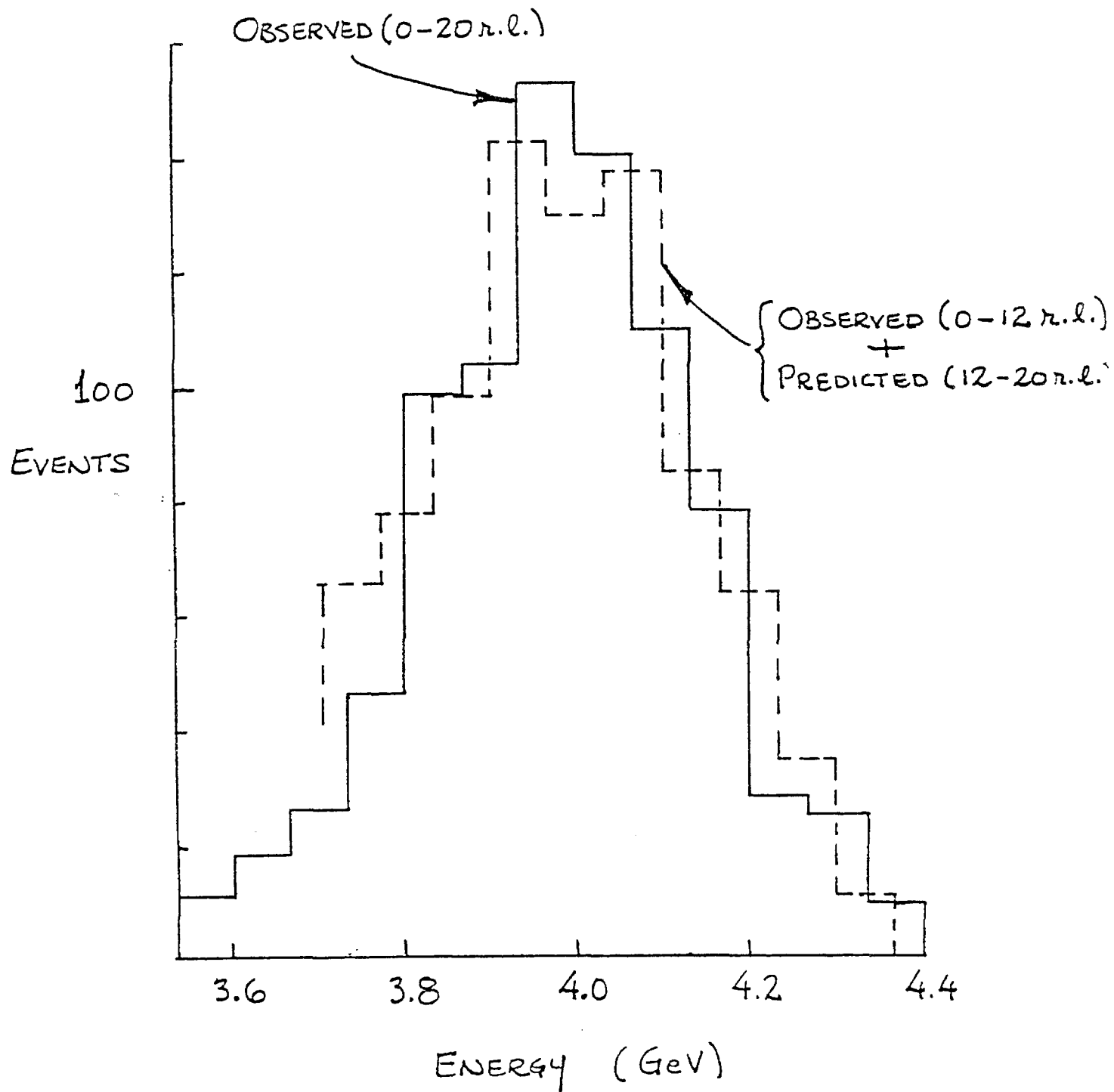


Figure I-8

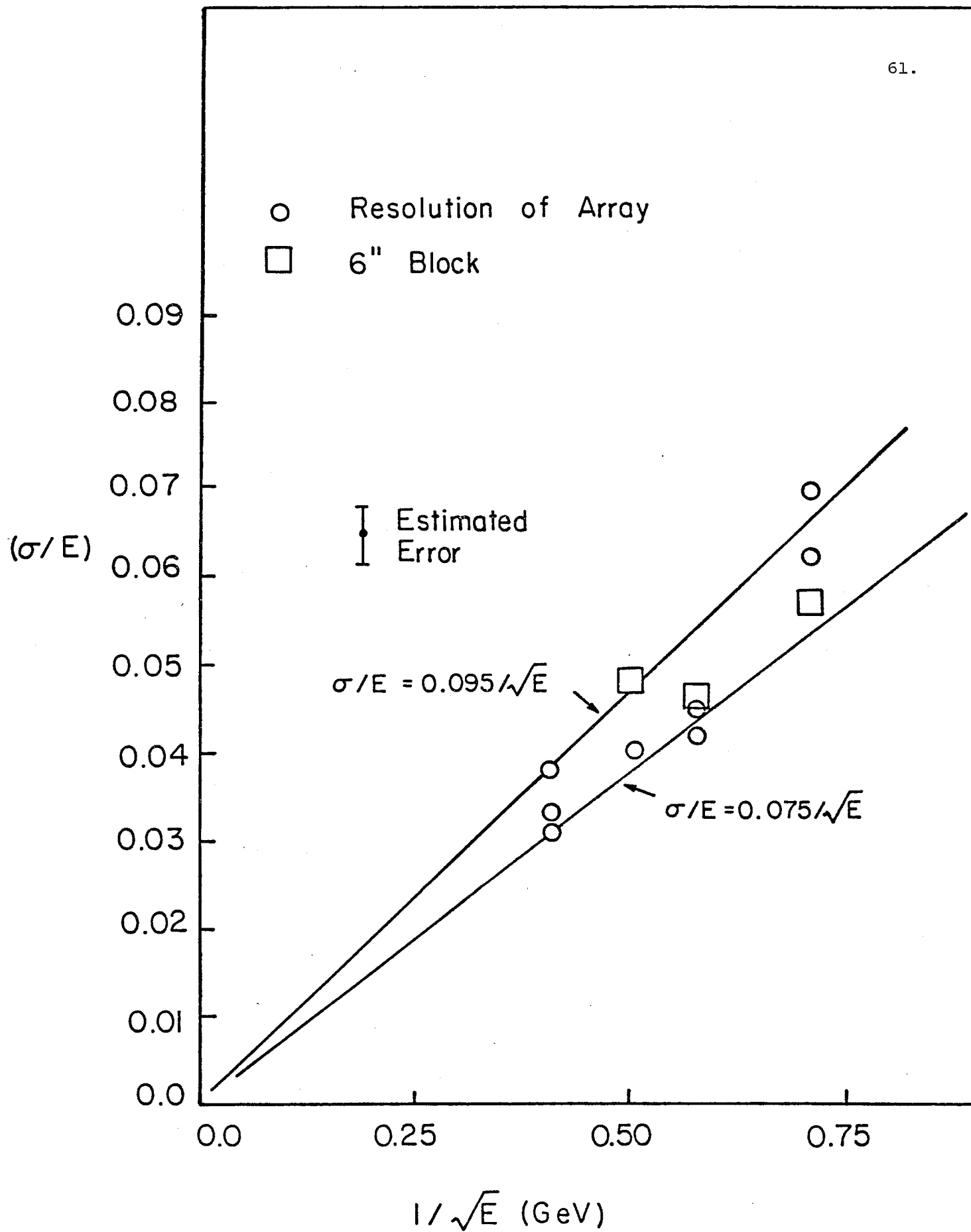


Figure I-9 Energy Dependence of Resolution

In order to test an array of bars in the appropriate energy range for LAPDOG, we have assembled a test calorimeter consisting of 5 (transverse) by 12 (longitudinal) bars of dimension $6.5 \times 6.5 \times 140 \text{ cm}^3$. These bars will be arranged in 12 layers, each staggered sideways by half a block to prevent any electrons from seeing a crack through the whole detector. This module will be inserted into a high energy electron beam at Fermilab in Spring 1982, together with various calibration systems under study.

The calibrations to be tested and cross-correlated include: 1) beam muons passing perpendicular to the long axes of the blocks, 2) cosmic ray muons passing nearly parallel to the long axes toward the phototubes, 3) Am^{241} - $\text{NaI}(\text{Tl})$ sources mounted on each bar, 4) fiber optics distribution of light distributed to each bar from both spark gap light and high intensity LED light, and 5) individual LED's mounted on each bar. The light distributed through fiber optics will also be monitored by a unit gain vacuum photodiode and by a reference phototube viewing the same fiber-distributed light and equipped with its own radioactive source. We plan further laboratory tests of alternative calibration sources including laser light and alternative radioactive sources.

The three chief goals of the Fermilab test are measurement of the energy resolution in the 50-100 GeV region, demonstration of a viable calibration method, and measurement of the hadron rejection factor for the LAPDOG array. We hope to study important factors, such as resolution variations as a function of incident particle angle and position in the presence of attenuation corrections. We also intend to determine the depth of the array required to get good resolution, using the individual shower profiles to predict leakage energy.

An important consideration for any lead glass based experiment is the possibility of darkening due to irradiation. Some information on radiation damage to lead glass by high energy particles exists⁸, but it is not very detailed. The CCR experiment at CERN, working with SF5 glass (of intrinsically higher lead content and shorter attenuation length), found that a 300 rad dose gives noticeable change in attenuation length. We estimate an average dose of 300 rad would accumulate in LAPDOG glass at the collider in 10 years of running at $\mathcal{L} = 2 \times 10^{29} \text{ cm}^{-2} \text{ sec}^{-1}$. Thus radiation damage seems unlikely to be a major problem, given reasonably clean beam conditions and low background radiation from the main ring during injection. However, owing to the potential seriousness of the radiation damage problem, we have embarked on a measurement of transmission changes in F2 glass after known irradiations near a beam dump at Brookhaven. We should point out that the LAPDOG arrangement of glass bars is less susceptible from darkening than the conventional (end-on) arrangement. This is because we are capable of monitoring attenuation factors throughout the experiment using straight-through particles and making the required correction. In the conventional arrangement, increase in attenuation length directly affects resolution through the unavoidable fluctuations in longitudinal shower development.

It must be clear that, while tests of an extruded lead glass bar detector have shown it to be an extremely powerful device, many further tests and refinements remain to be made. Some of these involve the glass manufacture itself - comparison of glasses of different content, including the possibility of Cerium doped glass to improve its radiation resistance. (Cerium lead glass is used for windows of viewing ports to high radiation areas.) To date, we

have used bars polished on phototube and mirror ends; preliminary tests show that rough-ground surfaces, wetted with optical cement will give similar light collection and allow further cost savings.

The use of filters to remove blue light make light collection more uniform and could reduce the stringency of attenuation corrections. Photocathode response should also be optimized to collect the maximum Cerenkov light. Long term stability of calibration systems needs to be studied. All of these optimizations will serve to improve the detector, enhance its ease of operation or reduce its cost. The basic utility of the technique has however been demonstrated by the testing program already completed.

LETTERS TO THE EDITOR

LOW COST LEAD GLASS CHERENKOV DETECTORS

P.D. GRANNIS, D. JAFFE and M.D. MARX

State University of New York, Stony Brook, New York, U.S.A.

Received 18 February 1981

We have compared the optical properties of lead glass bars of three different surface qualities. One was ground and polished in the conventional manner; the other two were in the unimproved state resulting from the extrusion or casting process. We find that the three bars exhibit similar optical characteristics. Use of such unpolished lead glass Cherenkov bars in electromagnetic shower detectors should result in considerable cost savings.

The use of lead glass blocks for electromagnetic shower measurements has been widespread in high energy physics experiments over the past decade. The small radiation length and the visibility of the full shower development made lead glass one of the most precise detectors for electron and photon energy measurements. However, the relatively high cost of lead glass has precluded its universal use. A major share of the cost of standard lead glass blocks or bars appears to be due to the surface preparation; typically a raw block, cast or extruded from a molten state, is mechanically cut, ground and polished to produce sharp corners and optically flat surfaces. We have performed tests on three bars of lead glass; one was polished in the usual manner and the others were used as supplied from the extrusion or extrusion casting processes with only the small end surface cut and polished. We find that the optical characteristics of all three are virtually the same. Thus we envision the possibility that for many applications, where mechanical tolerances can be relaxed, a factor of two or more in cost saving can be realized.

The three bars are shown in fig. 1. An extruded bar of F-2 lead glass from Schott Optical Glass [1] was cut into two pieces. One half was polished on the ends only and yielded the piece, labeled extruded, of dimension $66 \times 66 \times 600 \text{ mm}^3$. The other half was ground and polished on all surfaces; this polished piece was $58 \times 58 \times 599 \text{ mm}^3$. The extrusion cast piece was Ohara Glass [2] F2WS and had dimension $64 \times 72 \times 608 \text{ mm}^3$.

The extruded piece shows a fairly regular ripple pattern on all four transverse sides with amplitude

about $1/5 \text{ mm}$ and a spacing of about 4 mm . The surfaces appear to be quite smooth on the scale of optical wavelengths. The extrusion cast piece has three relatively flat surfaces; the fourth has an irregular rippling of amplitude about $1/3 \text{ mm}$ and spacing between 3 mm and 10 mm . There appear to be more blemishes on this surface than on the other three. The three flat surfaces are cooled in contact with an extrusion mold, while the fourth surface cools in contact with air causing the "chill" marks.

We have tested these pieces in an unseparated beam of $4 \text{ GeV}/c$ particles (mainly pions) at the Brookhaven National Laboratory AGS. The beam was defined by three scintillation counters (two before the lead glass bar and one behind); the beam definition at the bar was 25.4 mm (vertical) \times 12.7 mm (horizontal). The requirement of a count in the scintillator following the bar served to suppress interactions within the bar, so the source of light was dominantly Cherenkov light from single relativistic particles. The lead glass bars were viewed by a single Amperex 56DVP photomultiplier tube at one end. The tube was spring loaded against the bar with no optical grease or cement; the same tube was used for all three bars. The bars were loosely wrapped with opaque black plastic for light sealing; there was no evidence of any optical contact between sides or ends of the bar and the wrapping.

Measurements were taken with several orientations of the lead glass bars relative to the beam direction. Fig. 2 shows the distribution of the pulse areas observed with the beam directed down the long axis of the bars. In this orientation, triggering particles are

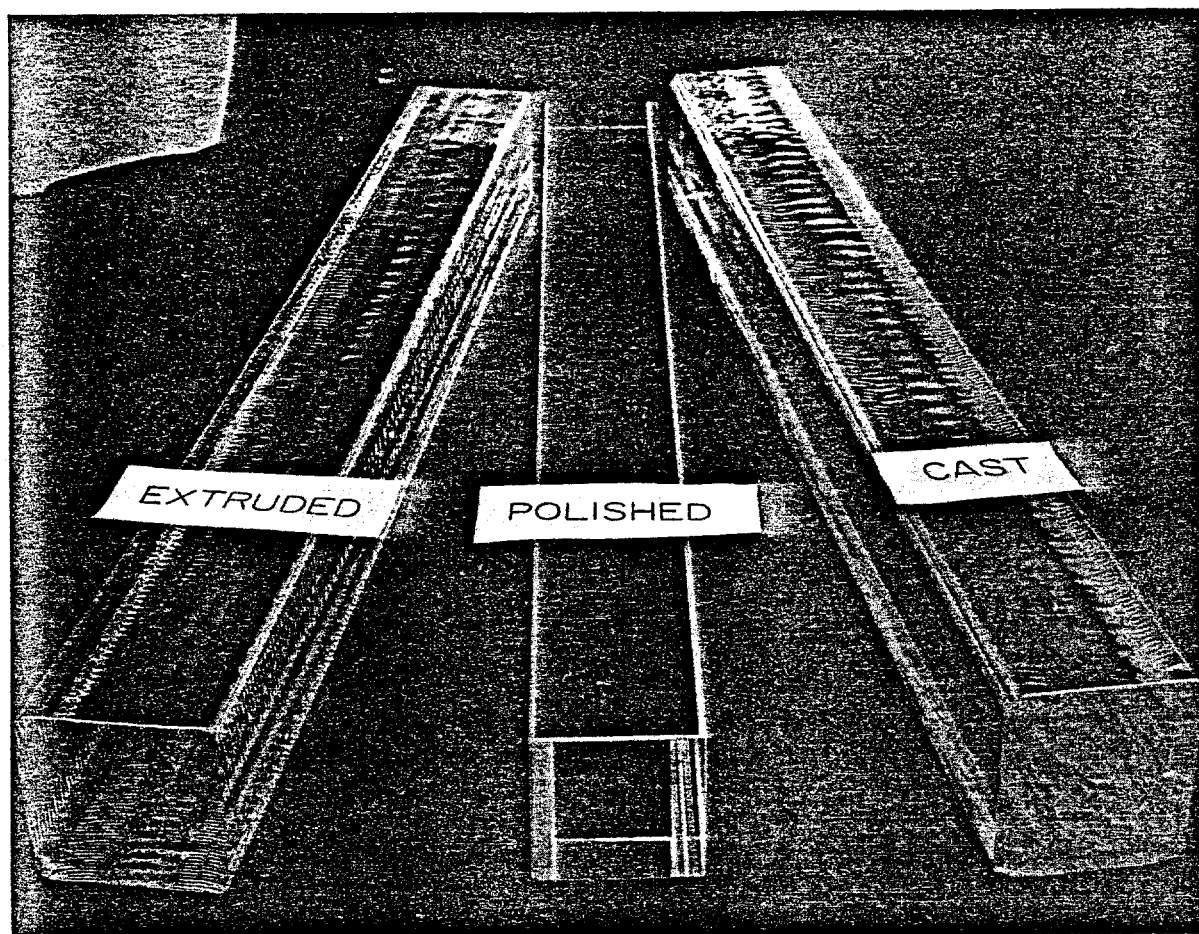


Fig. 1. The three lead glass bars tested.

mainly muons due to the high probability of hadronic scattering in 60 cm of glass. We note that this orientation critically tests the optical surface properties of all four transverse sides, as Cherenkov light generated from the upstream end makes multiple reflections at all side walls. To within the errors of system gain calibration for the various measurements, the positions and widths of the peaks are the same for the three bars. Fig. 3 shows the distribution of pulse areas for the beam directed perpendicular to the long axis. Again we observe that the three bars are essentially alike.

We have measured the light yield observed as a function of a distance between the photomultiplier face and the beam, for normal incidence. Fig. 4 shows the dependence of the mean pulse area with distance, after correction for the different Cherenkov radiator thickness and the different fractions of end area

sampled by the photomultiplier. Apart from a gentle fall off in light yield as the distance increases from 0 to 100 mm, there is little distance variation. We infer that the intrinsic attenuation length of the lead glass for the wavelength band of our photomultiplier is ≥ 5 m, with no significant difference among the three samples tested.

Finally, we have examined the dependence of the light yield upon the angle of beam incidence. Fig. 5 shows this angular variation for polished and extruded bars; an angle of 0° denotes the beam is perpendicular to the long axis of the bar and positive angles result when the beam is tending to point toward the photomultiplier. The data of fig. 5 are normalized to fixed radiator length and phototube area sampling fraction. We observe similar response from both bars. We see that for the beam pointing away from the tube, there is little variation of yield

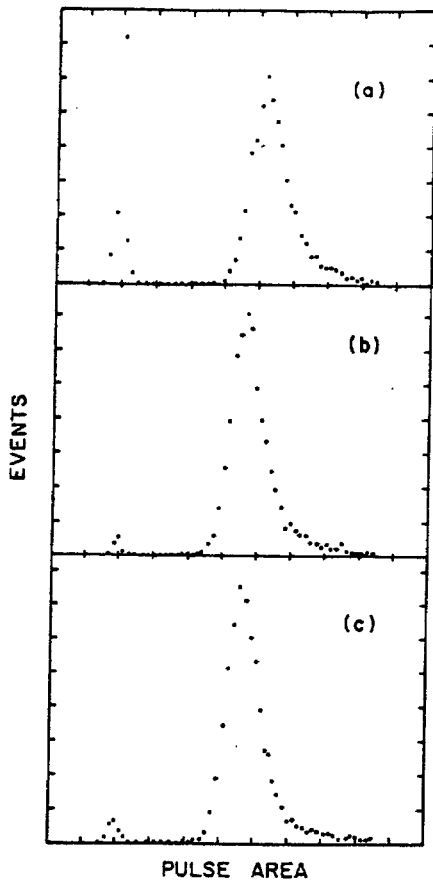


Fig. 2. Number of events versus pulse area with the beam directed along the axis of the bars. The peak at small pulse area occurs for triggers with no accompanying light in the lead glass (pedestal). Curves (a), (b) and (c) are for polished, extruded, and extrusion cast bars.

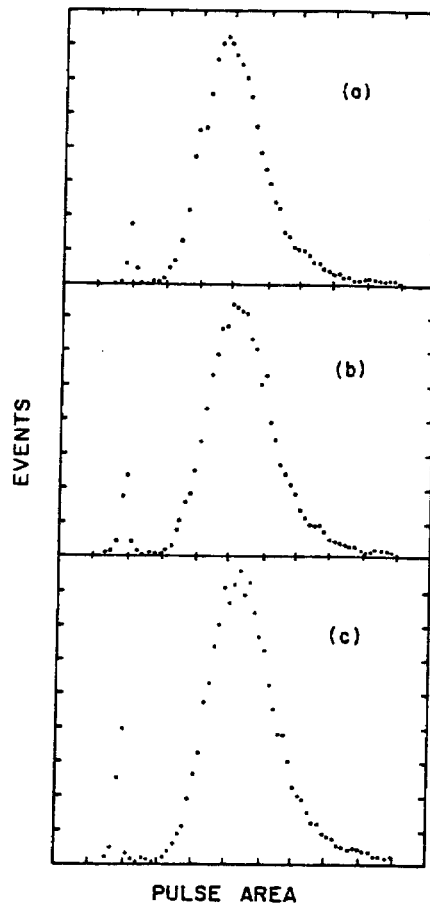


Fig. 3. Number of events versus pulse area with the beam directed perpendicular to the long axis of the bars. The peak at small pulse area occurs for triggers with no accompanying light in the lead glass (pedestal). Curves (a), (b), and (c) are for polished, extruded, and extrusion cast bars.

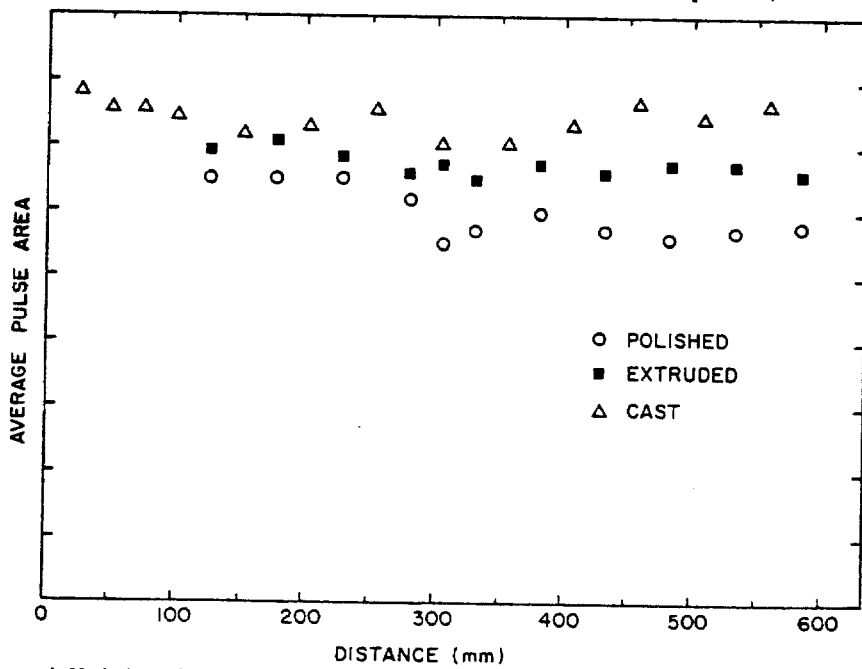


Fig. 4. Variation of average pulse area with distance of the beam from the photomultiplier.

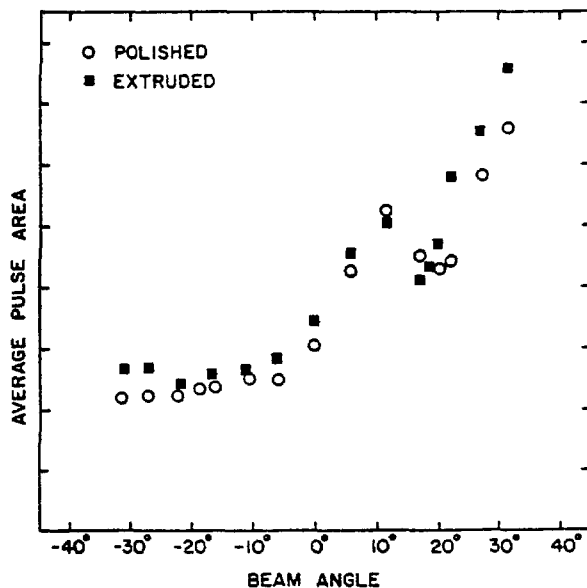


Fig. 5. Variation of average pulse area with angle of the beam direction.

with angle. When the beam direction points more directly toward the tube, the gain increases as expected since the Cherenkov cone is more completely within the total internal reflection regime. However, we note a significant dip in the yield around $\theta = 20^\circ$ which was unexpected; this dip occurs from both polished and extruded bars, but at slightly different angles. We have investigated this effect with a simple Monte Carlo calculation in which Cherenkov light is generated and representative rays are traced through the multiple reflections to the

photomultiplier. We find that in our geometry there are two components of light received at the tube; those rays which have been reflected from the far surface and those emitted toward the tube. The set of rays reflected from the far surface must bounce many times from the side surfaces. When the particle direction exceeds $\theta \approx 20^\circ$, there are no such rays in the Cherenkov cone which are capable of total internal reflection and the contribution of back reflected rays becomes zero. The dip in yield near 20° is then to be interpreted as the cutoff in the retroreflected component of light. For the extruded block, with its variation of side surface normals, the loss of retroreflected rays should occur at somewhat smaller beam angle.

In summary, we have found that lead glass bars without any surface grinding and polishing exhibit the same efficiency for Cherenkov light collection as do polished bars. We estimate the resultant savings in cost, if such unprocessed bars are used in an electromagnetic calorimeter, to be at least a factor 2.

We have benefitted from useful discussions with S. Aronson and J. Kirz in this study. This work was supported in part by DOE Contract no. DEACO280ER10699 and NSF Contract no. PHY7916904A01.

References

- [1] Schott Optical Glass, Inc., York Ave., Duryea, PA 18642, U.S.A.
- [2] Recon Optical Glass, 10 Shawnee Drive, Watchung, NJ 07060, U.S.A.

References

1. W. J. Marciano and Z. Parsa, Cornell Z⁰ Theory Workshop, CLNS 41-485 (Feb. 1981), p. 127.
2. S.D. Drell and T.M. Yan, Phys. Rev. Letters 25, 316 (1970).
3. D. Antreasyan et al., Phys. Rev. Letters 47, 12 (1981).
4. N.D. Giokaris et al., Phys. Rev. Letters 47, 1690 (1981).
5. A.L.S. Angelis et al., Phys. Letters 94B, 106 (1980)
6. J.A. Appel et al., Nucl. Instr. and Methods, 127, 495 (1975).
7. C. Kourkemelis et al., Phys. Letters 91B, 475 (1980).
8. J.S. Beale et al., Nucl. Instr. and Methods, 117, 501 (1974).
9. J. Brau et al., SLAC-PUB-2773 (July 1981).
10. F. Binon et al., Nucl. Instr. and Methods 188, 507 (1981).
11. B. Powell et al., CERN preprint EP 81-144 (1981).
12. F. Paige, BNL Preprint BNL 27066 (1979).
13. C. Quigg, Rev. Mod. Phys. 49, 297 (1977).
14. T.K. Gaisser, F. Halzen, and E.A. Paschos, Phys. Rev. D15, 2572 (1977).
15. C. Kourkoumelis et al., Phys. Letters 91B, 481 (1980).
16. I. Hinchliffe and R.L. Kelly, LBL preprint, LBL-12274 and CDF-83 (1981).
17. B. Winstein, private communication.
18. Reiter and Sengle, Nucl. Instr. and Methods 169, 469 (1980).
19. For example, HP 4558 have been used under routine conditions to provide 2×10^5 photoelectrons per tube (~ 25 GeV equivalent per block) to 20 phototubes simultaneously through fiber optics and with a 2.5% FWHM.
20. BNL-Brown-Japan-Pennsylvania-Stony Brook detector at BNL for neutral current studies with neutrinos. It contains 4000 phototubes, 13,000 proportional drift tubes in 200 tons of scintillator. It has been fully operational for the past year under computer control.

21. We use ISAJET, a code developed by F. Paige and S. Protopopescu of Brookhaven National Laboratory. ISAJET is based upon educated guesses of structure functions and hadron evolution functions, as well as p_T -smearing effects.

We are grateful to Mr. George Booth for his unique contribution to **this** proposal.